

Polyoxovanadates with ethylidene-pyridine functionalized bisphosphonate ligands: Synthesis, Structure, Spectroscopic Characterization, Magnetic and Anti-Bacterial studies

Dewendra Thakre,^a Sk Rajab Ali,^b Sakshi Mehta,^c Noohul Alam,^d Masooma Ibrahim,^e Debajit
Sarma,^{*d} Abhishake Mondal,^c Mrinmoy De,^b and Abhishek Banerjee^{*a}

a: Department of Chemistry, Visvesvaraya National Institute of Technology, Nagpur, India

b: Organic Chemistry Department, Indian Institute of Science, Bangalore, India

c: Solid State and Structural Chemistry Unit, Indian Institute of Science, Bangalore, India

d: Department of Chemistry, Indian Institute of Technology Patna, Patna, India

e: Institute of Nanotechnology, Karlsruhe Institute of Technology, Karlsruhe, Germany

KEYWORDS: Bisphosphonate, Polyoxovanadates, Infrared spectroscopy, Magnetic studies,
Anti-bacterial studies.

ABSTRACT

Reaction of ethylenepyridyl-functionalized bisphosphonates with vanadium containing oxo compounds has afforded three different bisphosphonate-polyoxovanadate derivatives, viz. $[(V^{IV}O_2)(V^V_2O_5)_2\{O_3P-C(O)(CH_2-2-C_5NH_4)-PO_3\}]^{10-}$ (**1**), $[(V^{IV}O_2)(V^V_2O_5)_2\{O_3P-C(O)(CH_2-3-C_5NH_4)-PO_3\}_2]^{10-}$ (**2**), $[(V^{IV}O)_3(O)\{O_3P-C(OH)(CH_2-4-C_5NH_4)-PO_3\}_3]^{8-}$ (**3**), obtained in aqueous ammonium acetate buffer solutions (pH 4.7). Polyanions **1** and **2** were synthesized by the reaction of V_2O_5 with 1-hydroxy-2-(2-pyridyl) ethylidene-1,1-bisphosphonic acid (**L1**) and 1-hydroxy-2-(3-pyridyl) ethylidene-1,1-bisphosphonic acid (**L2**), respectively. Polyanion **3** was obtained by the reaction of $VOSO_4$ with 1-hydroxy-2-(4-pyridyl) ethylidene-1,1-bisphosphonic acid (**L3**), in the presence of pyrazine. Single crystal X-ray diffraction and elemental analysis reveal that all the polyanions are crystallized as ammonium salts, $(NH_4)_4[H_6(V^{IV}O_2)(V^V_2O_5)_2\{O_3P-C(O)(CH_2-2-C_5NH_4)-PO_3\}_2]\cdot 9H_2O$ (**1a**), $(NH_4)_4[H_6(V^{IV}O_2)(V^V_2O_5)_2\{O_3P-C(O)(CH_2-3-C_5NH_4)-PO_3\}_2]\cdot 8H_2O$ (**2a**), $(NH_4)_2[H_6(V^{IV}O)_3(O)\{O_3P-C(OH)(CH_2-4-C_5NH_4)-PO_3\}_3]\cdot 26H_2O$ (**3a**), respectively. Polyanions **1** and **2** crystallize in the non-centrosymmetric space group $P2_12_12$ and have an S-shaped assembly containing two different sets of vanadium atoms, based upon their oxidation-state and different coordination environments. Polyanion **3** crystallizes in the centrosymmetric trigonal space group $R\bar{3}c$ and is observed to have a highly symmetric trinuclear structure. The polyanions have been characterized in solution with 1H and ^{31}P NMR, and optical spectroscopy, and in the solid state with detailed magnetic analysis. The magnetic studies under an external dc field showed paramagnetic behavior in agreement with the presence of V(IV) ions for **1a-3a**. Furthermore, *in vitro* studies of the synthesized bisphosphonate-polyoxovanadate compounds were observed to exhibit peroxidase like activity, and hence were employed to enhance the antibacterial activity of H_2O_2 solution at very low concentrations thereby minimizing the

possibilities of other side effects. Isostructural derivatives of compounds **1a** and **2a** with **L3**, *viz.* $(\text{NH}_4)_4[\text{H}_6(\text{V}^{\text{IV}}\text{O}_2)(\text{V}^{\text{V}}_2\text{O}_5)_2\{\text{O}_3\text{P}-\text{C}(\text{O})(\text{CH}_2-4-\text{C}_5\text{NH}_4)-\text{PO}_3\}_2]\cdot 11\text{H}_2\text{O}$ (**4a**), has been identified using infrared spectroscopy, and characterized with NMR spectroscopy and elemental analysis. Similarly, an isostructural derivative of **3a** with **L2**, *viz.* $(\text{NH}_4)_2[\text{H}_6(\text{V}^{\text{IV}}\text{O})_3(\text{O})\{\text{O}_3\text{P}-\text{C}(\text{OH})(\text{CH}_2-3-\text{C}_5\text{NH}_4)-\text{PO}_3\}_3]\cdot 21\text{H}_2\text{O}$ (**5a**), has also been identified using infrared spectroscopy, and characterized with elemental analysis.

1. INTRODUCTION

Polyoxometalates with their diverse structure and properties have emerged as one of the predominant class of inorganic materials with a wide range of applications, especially in the fields of catalysis, magnetism, medicine, among others.¹⁻⁴ Majority of the conventional heteropolyoxometalate structures reported in the literature are built upon the Keggin and the Wells-Dawson class of polyanions; involving the heteroatom in closely encapsulated assemblies, wherein its role in such structures is predominantly structural.⁵⁻⁶ Recently, a new class of heteropolyoxometalate structures based upon the bisphosphonate moiety have been reported in the literature.⁷⁻⁹ In sharp contrast to the conventional polyoxometalate structures, such compounds usually exhibit an open structure-type with the ditetrahedral hetero group(s) situated on the outside of the polyanion structure.¹⁰⁻¹¹ These structural features allow for the tuning of the properties of the polyanions such as stability, solubility and polarity by modifying the nature or substituent of the hetero groups within the bisphosphonate ligands.

Bisphosphonate molecules, with the general formula $\text{H}_2\text{O}_3\text{P-C}(\text{R}_1)(\text{R}_2)\text{-PO}_3\text{H}_2$, are known therapeutic drugs having potential medical applications mainly towards the treatment of bone resorption disease and also exhibit antitumor activity.¹²⁻¹⁹ Such molecules are involved in stimulation of $\gamma\delta$ T cells which is the first line of defense against many of the pathogenic organisms, and are also active towards tumor cell arresting and surveillance.²⁰ The bisphosphonate assembly is structurally analogous to pyrophosphate (P_2O_7)⁴⁻ wherein the central oxygen atom is replaced by carbon atom, which becomes essential in providing resistance towards chemical and enzymatic hydrolysis. Researchers have developed a variety of bisphosphonates with substitution upon the methylene group to enhance their activity. The modification of the appendage R_1 and R_2 groups have allowed for the tailoring of biological and physiological properties.²¹ R_1 which is

predominantly a hydroxyl group has an affinity for Ca^{2+} ions,²²⁻²³ and R_2 is an aliphatic hydrocarbon chain or aromatic ring. Bisphosphonates containing heteroatomic aromatic ring(s) have been observed to be more potent than aliphatic hydrocarbon chains.²⁴⁻²⁵

As mentioned earlier, bisphosphonate-polyoxometalates have found a niche among the wider range of polyoxometalate literature with several interesting properties investigated, including magnetism, activity against HIV reverse transcription, and anti-cancer studies.²⁶⁻²⁷ The literature of bisphosphonate-polyoxometalates essentially began with the report of the dodecameric polyoxotungstate $[(\text{O}_3\text{P}-\text{CH}_2-\text{PO}_3)_4\text{W}_{12}\text{O}_{36}]^{16-}$ with methylene diphosphonate, by Kortz and Pope in 1994.²⁸ Subsequent to this, the literature of such compounds grew rapidly with the first reports of methylenediphosphonate-based molybdates²⁹ and functionalized-methylenediphosphonate with tungstates.³⁰ In many bisphosphonate-polyoxomolybdate assemblies presence of the $\{\text{Mo}^{\text{VI}}_3\text{O}_8\}$ unit is commonly observed, with derivatives reported of 1-hydroxyethane-1,1-bisphosphonate,³¹⁻³² 4-amino-1-hydroxy-butane-1,1-bisphosphonate,³³ 1-hydroxy-2-(pyridine-3-yl)ethane-1,1-bisphosphonate.³⁴ Mialane and coworkers introduced the $\{\text{Mo}^{\text{V}}_2\text{O}_4\}$ unit(s) into bisphosphonate-polyoxometalate assemblies, resulting in a range of compounds with either fully reduced³⁵⁻³⁷ or mixed-valent molybdates containing a range of bisphosphonates.³⁸⁻³⁹ Derivatives of such polyoxomolybdate-bisphosphonates containing the $\{\text{Mo}^{\text{V}}_2\text{O}_4\}$ unit have also been reported with 2,2,2-trifloro-1-hydroxyethane-1,1-,⁴⁰ 1-hydroxy-2-(pyridine-3-yl)ethane-1,1-bisphosphonate.⁴¹ Reports are also present of mixed-metal bisphosphonate-polyoxometalates containing the dimeric $\{\text{Mo}^{\text{V}}_2\text{O}_4\}$ unit with several 3d-block transition metals, such as vanadium(IV),⁴² chromium(III),⁴³ manganese(II),²⁷ iron(II),⁴⁴⁻⁴⁵ cobalt(II) and nickel(II),⁴⁶⁻⁴⁷ containing 1-hydroxyethane-1,1-bisphosphonate,⁴⁵⁻⁴⁶ 4-amino-1-hydroxy-butane-1,1-bisphosphonate,⁴² 1-hydroxy-4-((pyridin-2-ylmethyl)amino)butane-1,1-

bisphosphonic,⁴³ 1-hydroxy-2-(imidazol-1-yl)ethane-1,1-bisphosphonate or its derivatives,^{27, 44} and 1-hydroxy-2-(pyridine-3-yl)ethane-1,1-bisphosphonate.⁴⁷ Recently, polyoxotungstate-bisphosphonates containing lacunary keggins-assemblies and with 3d-transition metals have also been reported. These include assemblies of $\{PW_9O_{34}\}^{9-}$ with cobalt(II) and 1-hydroxy-4-((pyridin-2-ylmethyl)amino)butane-1,1-bisphosphonic acid,⁴⁸ 4-(bis(pyrid-2-ylmethyl)amino)-1-hydroxybutane-1,1-bisphosphonic acid,⁴⁸ 1-hydroxy-4-((thiophen-3-ylmethyl)amino)butane-1,1-bisphosphonic acid,⁴⁹ or 4-amino-1-hydroxy-butane-1,1-bisphosphonate,⁵⁰ of $\{PW_9O_{34}\}^{9-}$ or $\{SiW_9O_{34}\}^{10-}$ with nickel(II) and 4-amino-1-hydroxy-butane-1,1-bisphosphonate⁵¹⁻⁵² or 1-hydroxy-4-(naphthalen-1-ylmethyl)aminobutane-1,1-diphosphonic acid;⁵³ and of $\{SiW_9O_{34}\}^{10-}$, $\{SbW_9O_{33}\}^{9-}$ or $\{P_2W_{15}O_{56}\}^{12-}$ with copper(II) and 4-amino-1-hydroxy-butane-1,1-bisphosphonate.⁵⁴ Mixed-metal lanthanide derivatives with $\{AsW_9O_{33}\}^{9-}$ and containing 1-hydroxyethane-1,1-bisphosphonate have been reported with Ce, Nd, Sm and Eu.⁵⁵

Despite the growing literature of bisphosphonate-polyoxometalates, reports of exclusive bisphosphonate-polyoxovanadates are extremely few. So far the only reports of such compounds contain the mixed-valent V(IV)/V(V) assemblies of $[(V_5O_9(OH)_2(H_2O)\{O_3P-C(R)(O)-PO_3\}_2)]^{4-}$ with 4-amino-1-hydroxy-butane-1,1-bisphosphonate ($R = C_3H_6NH_3$),⁵⁶ 1-hydroxy-2-(imidazol-1-yl)ethane-1,1-bisphosphonate ($R = -C_4N_2H_5$);⁵⁶ and $[(V_6O_{10}(H_2O)_2\{O_3P-C(C_3H_6NH_3)(O)-PO_3\}_4)]^{8-}$ with 4-amino-1-hydroxy-butane-1,1-bisphosphonate;⁵⁶ as well as the trimeric assembly of V(IV) atoms only, $[\{V_3(H_2O)O_3\}\{O_3P-C(OH)(R)-PO_3\}_3]^{n-}$ with 1-hydroxyethane-1,1-bisphosphonate ($R = -CH_3$, $n = 6$),⁵⁷⁻⁵⁹ 1-hydroxy-2-(imidazol-1-yl)ethane-1,1-bisphosphonate ($R = -C_4N_2H_5$, $n = 3$),⁵⁶ and 4-amino-1-hydroxy-butane-1,1-bisphosphonate ($R = -(CH_2)_2CH_2NH_2$, $n = 3$),⁶⁰ respectively. This is surprising considering the tremendous potential of vanadium as

versatile redox species as well as its role as an essential element in several bio-inorganic catalytic processes.

In order to further investigate upon this hitherto mainly unexplored area of bisphosphonate-polyoxovanadate chemistry and look for potentially newer applications of such compounds, we studied the reaction of vanadium with the pyridinyl-based aromatic bisphosphonate species, *viz.* 1-hydroxy-2-(2-pyridyl) ethylidene-1,1-bisphosphonic acid (**L1**), 1-hydroxy-2-(3-pyridyl) ethylidene-1,1-bisphosphonic acid (**L2**), and 1-hydroxy-2-(4-pyridyl) ethylidene-1,1-bisphosphonic acid (**L3**), respectively. The presence of the heteroaromatic functional group upon the bisphosphonate moiety provides us with an additional functionality to explore from, namely the location of the heteroatom upon the aromatic ring. Herein we report our observations upon the reactivity of such pyridine-based bisphosphonate molecules with different vanadium containing oxo compounds, isolation of five new bisphosphonate-polyoxovanadate derivatives, their thorough characterization in solution and solid-state. Apart from the structurally characterized polyanions from single-crystal X-ray diffraction, analogous derivatives for which single crystals were not obtained have been identified using Infrared Spectroscopy method and characterized with elemental analysis. Spectroscopic and magnetic studies have been performed to study the properties of the polyanionic structures. Furthermore, we have explored the peroxidase like catalytic activity of prepared complexes. The observed peroxidase-like activity of the isolated polyoxovanadate compounds were implemented for the *in vitro* antibacterial studies against methicillin-resistant *staphylococcus aureus* (MRSA) bacterial strain. The result showed the enhanced antibacterial activity in presence of the synthesized compounds with very low concentration of H₂O₂ (0.5 mM); making it suitable for biological applications.

2. RESULTS AND DISCUSSION

2.1 SYNTHESIS AND STRUCTURE

Upon the successive reaction of several vanadium containing oxo compounds (vanadium pentoxide and vanadium oxosulfate) with the three bisphosphonate ligands of interest (**L1**, **L2** and **L3**), under varying conditions, three sufficiently pure compounds in crystalline phase were isolated. All three compounds were synthesized upon the reaction of vanadium precursor(s) with the respective bisphosphonate ligand in ammonium acetate buffer (pH 4.7) and isolated as ammonium salts, $(\text{NH}_4)_4[\text{H}_6(\text{V}^{\text{IV}}\text{O}_2)(\text{V}^{\text{V}}_2\text{O}_5)_2\{\text{O}_3\text{P}-\text{C}(\text{O})(\text{CH}_2-2-\text{C}_5\text{NH}_4)-\text{PO}_3\}_2]\cdot 9\text{H}_2\text{O}$ (**1a**), $(\text{NH}_4)_4[\text{H}_6(\text{V}^{\text{IV}}\text{O}_2)(\text{V}^{\text{V}}_2\text{O}_5)_2\{\text{O}_3\text{P}-\text{C}(\text{O})(\text{CH}_2-3-\text{C}_5\text{NH}_4)-\text{PO}_3\}_2]\cdot 8\text{H}_2\text{O}$ (**2a**), $(\text{NH}_4)_2[\text{H}_6(\text{V}^{\text{IV}}\text{O})_3(\text{O})\{\text{O}_3\text{P}-\text{C}(\text{OH})(\text{CH}_2-4-\text{C}_5\text{NH}_4)-\text{PO}_3\}_3]\cdot 26\text{H}_2\text{O}$ (**3a**), respectively. Compounds **1a** and **2a** are synthesized by the reaction of vanadium pentoxide with 1-hydroxy-2-(2-pyridyl) ethylidene-1,1-bisphosphonic acid (**L1**) and 1-hydroxy-2-(3-pyridyl) ethylidene-1,1-bisphosphonic acid (**L2**), respectively. Interestingly, compound **3a** was obtained upon the reaction of vanadium oxysulfate with 1-hydroxy-2-(4-pyridyl) ethylidene-1,1-bisphosphonic acid (**L3**) in the presence of pyrazine. Pyrazine itself was not observed to be present in the structure of the isolated compound but is essential for the formation of **3a**. The synthesized compounds were structurally characterized using single-crystal X-ray diffraction and their phase purity determined using powder X-ray diffraction method [**Figure S1**, **S2** and **S3** in Supporting Information], and elemental analysis. **1a** and **2a** were observed to crystallize in the non-centrosymmetric Orthorhombic space group of $P2_12_12_1$; while **3a** crystallizes in the centrosymmetric Trigonal space group of $R\bar{3}c$.

Polyanions **1** and **2** were observed to be isostructural with each other differing only in the orientation of the aromatic ring. Structural analysis using single-crystal X-ray diffraction reveals

that polyanions **1** and **2** have a twisted S-shaped structure wherein dimeric $\{V^V_2O_5\}$ units are connected with an octahedral $\{V^{IV}O_6\}$ via two bisphosphonate linkages at opposite sides [see **Figure 1(a)** and **1(b)**]. The asymmetric unit of polyanion **1** and **2** consists of total five vanadium atoms each, with V(1) in +4 oxidation state and V(2), V(3), V(4), V(5) in +5 oxidation state based on bond valence sum calculations [see Supporting Information **Table S1** and **S2**]. The bisphosphonate units are connected via the P-O-V as well as C-O-V linkages. The two bisphosphonate units in each polyanion structure are oriented in oppositely directing faces. For these two polyanions, the idealized point-group symmetry can be considered to be C_{2v} . The orientation of the aromatic ring in the solid-state assembly is directed by the dipolar, $\pi\dots\pi$ as well as hydrogen-bonding interactions (*vide-infra*). With an inter-ring distance of 3.5 – 4.5 Å, such $\pi\dots\pi$ stacking interactions are expected to have significant effects upon the arrangement of the polyanions as well as the functional group(s) on the bisphosphonate moiety, in the solid-state. Such an S-shaped structure closely resembles the structure of the polyanions reported previously obtained with 1-hydroxy-2-(imidazole-1-yl)ethane-1,1-diphosphonic acid, reported by Mialane and coworkers.⁵⁶

Polyanion **3** has a highly symmetrical triangular structure consisting of three alternately connected $\{V^{IV}O_6\}$ units with three bisphosphonate ligands [see **Figure 2**]. In keeping with the high symmetry space group of **3a**, the asymmetric unit of polyanion **3** was observed to consist of only one vanadium atom, V(1), in +4 oxidation state, based on bond valence sum calculations [see Supporting Information **Table S3**], and one bisphosphonate moiety. Unlike polyanions **1** and **2**, in polyanion **3** only P-O-V linkages are observed to be present with the hydroxyl group bonded to the central carbon-atom of the bisphosphonate moiety remaining non-connected with any metal center. Most interestingly, the asymmetric unit and in extension the polyanion structure is observed

to consist of a centrally-located oxygen-atom connected to every vanadium atom via an unusually long V-O bond (bond distance 2.4598(4) Å). This particular oxygen-atom is observed to be located upon a three-fold axis of rotation and therefore has a 33.33% occupancy in the asymmetric unit. The polyanion therefore can be attributed to have an idealized point-group symmetry of D_{3h} . Akin to this centrally located oxygen-atom; three more atoms, assigned to as two counter-cations (one above and another below the plane of the polyanion) and one water molecule, are also observed to be located on the 3-fold axis of rotation and thus having a 33.33% occupancy in the asymmetric unit as well. Such a polyanion structure has been observed previously with 1-hydroxyethylidene-1,1-bisphosphonate,⁵⁷⁻⁵⁹ with 1-hydroxy-2-(imidazole-1-yl)-1,1-bisphosphonic acid,⁵⁶ and with 4-amino-1-hydroxy-butane-1,1-bisphosphonate.⁶⁰

2.1.1 Infrared Spectroscopic studies on isolated products from the reaction of vanadium(IV) and vanadium(V) containing oxo compounds with L1, L2 and L3

We have tried to assign vibrational peaks observed in the infrared spectra for compounds **1a**, **2a** and **3a** based upon literature references of vanadium oxo complexes and phosphonate groups [see **Figure 3**]. For both compounds **1a** and **2a**, the strong vibrational peaks at 1168 cm^{-1} and 1061 cm^{-1} can be associated with P=O and P-O stretching.⁵⁸ while the strong stretching vibrational peak(s) in the region 955 - 930 cm^{-1} can be attributed with V(IV)=O stretching.⁶¹ Peaks at 819 and 776 cm^{-1} can be attributed to the O-V-O vibration, whereas peaks at 741 cm^{-1} and 441 cm^{-1} are characteristic of bent mono-oxo-bridge V-O-V connectivity asymmetric vibrational band and a symmetric vibrational band, respectively. The P-C bond stretching vibration band is assigned at 635 cm^{-1} for both compounds **1a** and **2a**.

In case of compound **3a**, the peaks at 1100 cm^{-1} and 1061 cm^{-1} can be attributed to P=O and P-O stretching vibrations, respectively, and the strong vibrational peak in the region ~990 cm^{-1} can

be associated with the mono-oxo V(IV)-O functional group stretching vibration. The peak at 821 cm^{-1} can be attributed to the O-V-O bridge vibrational frequency $\nu_s(\text{O-V-O})$ for **3a**. The P-C bond stretching vibration can also be assigned to 635 cm^{-1} .

Having obtained three different crystalline-phase compounds with three different bisphosphonates, we embarked on further understanding the reactivity of different vanadium compounds with all three ethylenepyridinyl-functionalized bisphosphonate ligands. With structural and spectroscopic data of **1a**, **2a** and **3a** present, we tried to identify isostructural derivatives of S-shaped and triangular polyoxovanadates with **L1**, **L2** and **L3**; for which single crystals for structure determination could not be obtained. We therefore relied on a thorough infrared spectroscopic characterization upon all products isolated from the extensive reaction of V_2O_5 with **L3**; as well as from the reaction of VO_2 with **L1** and **L2**, for our analysis. A comparison of the infrared spectra of **1a**, **2a** and product obtained upon reaction of V_2O_5 with **L3**, showed a complete peak by peak match of all three samples [Figure 3(a) shows the fingerprint region of the infrared spectra for all three isolated products from the reaction of V_2O_5 with **L1** (**1a**), **L2** (**2a**) and **L3**, respectively. For the complete spectra see Figure S4 in Supporting Information]. This study confirmed the formation of an isostructural derivative of polyanions **1** and **2** with **L3** as well. The formula for the isostructural polyanionic compound of **1a** and **2a** was determined to be $(\text{NH}_4)_4[\text{H}_6(\text{V}^{\text{IV}}\text{O}_2)(\text{V}^{\text{V}}_2\text{O}_5)_2\{\text{O}_3\text{P-C(O)}(\text{CH}_2\text{-4-C}_5\text{NH}_4\text{-PO}_3\}_2]\cdot 11\text{H}_2\text{O}$ (**4a**) using elemental analysis studies. Therefore, for **4a**, in the infrared spectra, observed to be coincidental with **1a** and **2a**, the characteristic peaks for P=O and P-O stretching are at 1169 and 1060 cm^{-1} , respectively; for V(IV)=O stretching in the region of 950 – 930 cm^{-1} ; for O-V-O vibration at 832 cm^{-1} ; and for bent mono-oxo-bridge V-O-V vibrations at 746 and 445 cm^{-1} .

A similar comparative infrared spectral data of products obtained upon the extensive reaction of VOSO_4 with **L1** and **L2**, under varying conditions, and with **3a** showed a reasonable match of the spectra however between **3a** and product isolated with **L2** only [Figure 3(b) shows the fingerprint region of the infrared spectra for all three isolated products from the reaction of VOSO_4 with **L1**, **L2** and **L3** (**3a**), respectively. For the complete spectra see Figure S5 in Supporting Information]. The formula for the isostructural polyanionic compound of **3a** with **L2** was determined to be $(\text{NH}_4)_2[\text{H}_6(\text{V}^{\text{IV}}\text{O})_3(\text{O})\{\text{O}_3\text{P}-\text{C}(\text{OH})(\text{CH}_2-3-\text{C}_5\text{NH}_4)-\text{PO}_3\}_3]\cdot 21\text{H}_2\text{O}$ (**5a**) using elemental analysis studies. Therefore, from the infrared spectra of compound **5a**, coincidental with **3a**, the characteristic peaks are observed at 1115 and 1040 cm^{-1} for $\text{P}=\text{O}$ and $\text{P}-\text{O}$ stretching vibrations, respectively; at $\sim 990\text{ cm}^{-1}$ for mono-oxo $\text{V}(\text{IV})-\text{O}$ functional group stretching vibration; at 818 cm^{-1} to the $\text{O}-\text{V}-\text{O}$ bridge vibrational frequency $\nu_s(\text{O}-\text{V}-\text{O})$; and at 620 cm^{-1} for $\text{P}-\text{C}$ bond stretching vibration. Thus, even with extensive screening, no isostructural triangular assembly of $\text{V}(\text{IV})$ with the bisphosphonate ligand **L1** was obtained.

All compounds show characteristic peaks due to the presence of crystal waters and ammonium counterions. The broad vibrational peak at $\sim 3400\text{ cm}^{-1}$ and the sharp peak at $\sim 1600\text{ cm}^{-1}$ are the characteristic of stretching vibration of $(\text{O}-\text{H})$ and bending vibration of $(\text{O}-\text{H})$ in the lattice and coordinated water molecules, while the sharp peak at 1400 cm^{-1} can be ascribed for the $\text{H}-\text{N}-\text{H}$ stretching from the ammonium counterions.^{62, 63}

2.1.2 Weak Interactions and Crystal Packing

As is observed for most polyanionic assemblies, non-covalent interactions such as electrostatic and hydrogen-bonding, play a predominant role in the arrangement of the polyanions leading to the crystalline solid-state.⁶⁴ The assemblies of the polyanions and the cations in **1a**, **2a** and **3a** are no exception to this. However, for **1a**, **2a** and **3a**, in addition to the effect of electrostatic and

hydrogen-bonding interactions, π - π stacking as well as dipolar interactions, due to the presence of the aromatic pyridine rings, also play an important role towards determining the overall assemblies of the polyanions in the solid-state.

The compounds **1a** and **2a** crystallize in the non-centrosymmetric Orthorhombic space group $P2_12_12$ and **3a** crystallizes in the highly symmetric Trigonal space group $R\bar{3}c$, reflecting the overall symmetry of the polyanions. For **1a** and **2a** the packing of the ions in the solid-state is also observed to be very similar, except for the orientation of the aromatic rings.

The intermolecular hydrogen bonding present in these compounds is predominantly because of the presence of donor C–H groups, from heteroaromatic ring sp^2 -hybridized C–H bond, and the acceptor H–O groups, from the $\{V^V_2O_5\}$ unit, in the polyanions. The intermolecular hydrogen-bond distances between the donor and the acceptor atoms for compounds **1a** and **2a** are in the range of 3.090 Å - 3.320 Å [see **Table S4** in Supporting Information] and 3.06 Å - 3.93 Å [see **Table S5** in Supporting Information], respectively. The π - π staking (side-wise π - π overlap between two aromatic rings of two different polyanionic units) distance of separation between the two pyridine rings is 4.3474 Å and 3.4459 Å, for polyanions **1** and **2**, respectively. This range of 3.5 – 4.5 Å is ideal for such interactions to exist.⁶⁵⁻⁶⁶ The arrangements of the rings are also influenced by dipolar interactions between the C-N bonds, with the bonds being arranged exactly *anti* to each other in both **1a** and **2a** [see **Figure S6(a)** and **S7(a)**, respectively in Supporting Information].

Overall, in compounds **1a** and **2a**, the assembly of the ions in the solid-state are along the *a*-axis forming a one-dimensional chain [see **Figure S6(a)** and **S7(a)** for **1a** and **2a**, respectively in Supporting Information]. Two such chains form a dimeric arrangement. The dimeric arrangements of the one-dimensional chain are shown to form two distinct stacks which are

arranged in alternate arrangement along the *b*-axis resulting in the overall arrangement of the polyanions in the solid-state [see **Figure S6(b)** and **S7(b)** for **1a** and **2a**, respectively in Supporting Information].

For compound **3a**, apart from the symmetry of the crystal, hydrogen-bonding interactions are also observed to determine the overall packing of the ions in the solid-state. Due to the presence of a 3-fold axis, both in the crystal as well as in the polyanion, the polyanionic units are observed to arrange themselves in hexagonal packing arrangements along the *c*-axis [see **Figure S8** in Supporting Information]. Akin to **1a** and **2a**, for **3a**, inter-molecular hydrogen-bonds are also observed to be present between the donor C–H groups, from heteroaromatic ring sp²-hybridized C–H bond, and the acceptor H–O groups, from the {V^V₂O₅} unit, in the polyanions. The hydrogen-bond distances are in the order of 2.596 Å, 3.403 Å, 3.276 Å, 3.052 Å for the O1C1–H1C1···O3P1, C4–H4···O3P1 C6–H···O1P2 and C6–H6···O2P2, respectively [see **Table S6** in Supporting Information]. Thus, the presence of significant voids is observed in the solid-state arrangement of **3a**, occupied with water of crystallization and counter-cations. However, unlike **1a** and **2a**, wide separation distance between the aromatic rings indicates no substantial no π ... π stacking interactions for the compound **3a**.

2.1.3 Comparative study of Polyoxovanadate structures obtained with bisphosphonate ligands

As mentioned earlier and given that the number of reported structures of polyoxovanadate derivatives containing bisphosphonate ligands is still very low, iso-structural derivatives of **1** & **2**, and of **3**, respectively, with other bisphosphonate ligands have been reported in the literature. A comparison between such polyanionic assemblies reported earlier vs. the one reported in this article reveal some interesting features for such structures.

The structures and the parameters of the polyanions **1** and **2** can be compared with the ones obtained with 1-hydroxy-2-(imidazole-1-yl)ethane-1,1-bisphosphonate and 4-amino-1-hydroxybutane-1,1-bisphosphonate.⁵⁶ A comparative survey of all these polyanions, with respect to structure, bond-lengths and crystal symmetry, is provided in **Table 2**. Although the connectivity between the atoms within the polyanions $[(V_5O_9(OH)_2(H_2O)\{O_3P-C(O)(R)-PO_3\}_2)]^{4-}$ ($R = C_3H_6NH_3, C_4N_2H_5$), **1** and **2** are identical the orientation of the $\{V^V_2O_5\}$ units and functional group of the organic bisphosphonate moiety, in the solid state, is observed to depend upon the functional group itself. As such the S-shaped assembly similar with **1** and **2**, is observed with $[(V_5O_9(OH)_2(H_2O)\{O_3P-C(O)(C_3H_6NH_3)-PO_3\}_2)]^{4-}$, wherein the $\{V^V_2O_5\}$ units and two functional groups are oriented in opposite sides (*anti*-orientation). However, for $[(V_5O_9(OH)_2(H_2O)\{O_3P-C(O)(C_4N_2H_5)-PO_3\}_2)]^{4-}$ the $\{V^V_2O_5\}$ units and functional groups are now observed to orient along the same direction (*syn*-orientation), thereby forming a U-shaped structure. Since hydrogen-bonding interactions are observed for all these polyanions, the orientation of the functional groups within the polyanions is possibly influenced by other non-bonding interactions, such as the presence and/or absence of $\pi\dots\pi$ stacking interactions within the functional groups. With an interplanar distance in the range of 4.15 – 4.7 Å, significant $\pi\dots\pi$ stacking interactions between the imidazole groups are expected to be present between two properly oriented polyanion assemblies of $[(V_5O_9(OH)_2(H_2O)\{O_3P-C(O)(C_3H_6NH_3)-PO_3\}_2)]^{4-}$ (see previous section for a discussion of solid-state packing of polyanions **1** and **2**). Such interactions are clearly absent in $[(V_5O_9(OH)_2(H_2O)\{O_3P-C(O)(C_4N_2H_5)-PO_3\}_2)]^{4-}$, due to the absence of any aromatic functional group in the bisphosphonate ligand. We can therefore possibly infer that non-bonded interactions other than hydrogen-bonding, such as $\pi\dots\pi$ interactions, do play a significant role in the overall assembly of the structure of the polyanions in the solid-state.

Isostructural derivatives of polyanion **3** have been reported with 1-hydroxyethane-1,1-bisphosphonate,⁵⁷⁻⁵⁸ 1-hydroxy-2-(imidazole-1-yl)ethane-1,1-bisphosphonate⁵⁶ acid 4-amino-1-hydroxybutane-1,1-bisphosphonate.⁶⁰ A comparative survey of all these polyanions, with respect to structure, bond-lengths and crystal symmetry, is provided in **Table 3**. However, unlike polyanion **3**, the centrally located oxygen-atom in such structures is either observed to not bond equidistantly with the three vanadium-atoms^{56, 59} or bond with only one vanadium atom^{58, 60} (vanadium-oxygen bond distances ranging from 1.63 – 2.88 Å), thereby bringing asymmetry into the overall structure and/or the crystal. These polyanions are therefore observed to crystallize in the significantly low symmetry space-group(s) of *P-1*, *P2₁/c* and *P-1* for $[\{V_3(H_2O)O_3\}\{O_3P-C(OH)(CH_3)-PO_3\}_3]^{5-}$,⁵⁸ $[V_3O_3(H_2O)\{O_3P-C(OH)(C_4H_6N_2)-PO_3\}_3]^{3-}$,^{56, 58} and $[V_3O_3(H_2O)(O_3PC(C_3H_6NH_3)(OH)PO_3)_3]^{3-}$,⁶⁰ respectively. The symmetry or asymmetry within the structures can once again be possibly attributed to the symmetry of the functional group present within the bisphosphonate ligands. Unlike **3a**, wherein the bisphosphonate ligand is functionalized by the symmetrical 4-pyridinyl group, for the other reported polyanions such symmetry within the bisphosphonate ligand(s) is absent. This in all likelihood creates asymmetry within the polyanionic structure as well, leading to asymmetry in their three-dimensional arrangement within the crystal also.

2.2 SOLUTION PHASE MEASUREMENTS

The solution properties of all the compounds were studied with NMR and optical spectroscopy.

2.2.1 NMR Spectroscopic Studies

Multinuclear NMR studies of **1a**, **2a**, **3a**, **4a** and **5a** were performed in D₂O. The ¹H NMR peaks for polyanion **1**, **2** and **4** are observed to be extremely broad making the discerning of the coupling constants very difficult and the ³¹P NMR spectra containing a high degree of noise, ostensibly due

to its strong paramagnetic nature (*vide infra*). As such no solution-phase NMR spectra were observed for the strongly paramagnetic polyanions **3** and **5**, respectively, and no ^{51}V NMR was obtained for any of the polyanions.

The ^1H NMR of polyanion **1** shows the expected four peaks in the aromatic region and one peak in the aliphatic region. The polyanion **1** shows the following signals for the aromatic protons (values in parentheses for free bisphosphonate ligands): 8.62 (8.52), 7.68 (7.79), 8.42 (8.35) and 8.26 (7.90) ppm, for the positions 3, 4, 5, and 6 in the pyridine ring, respectively [see **Figure S9(b)** in Supporting Information]. Thus, the aromatic protons of polyanion **1** exhibits both downfield shifts of 0.1, 0.07, and 0.36 ppm for protons atom located at 3, 5, and 6 positions, respectively, and an upfield shift of 0.11 ppm for proton at 4-position, as compared to the free bisphosphonate (**L1**); which is predominantly due to the varying influence of the highly electronegative polyanion framework upon such protons. Furthermore, the polyanion **1** also exhibits the triplet peak for the aliphatic protons at 3.77 (3.57) ppm [see **Figure S9(c)** in Supporting Information], showing a downfield shift of 0.22 ppm, indicating a strong deshielding effect of the polyanion framework upon protons in close vicinity. Most interestingly, the $^3J_{\text{H-P}}$ coupling constant is observed to decrease from 12.5 Hz in the free bisphosphonate species **L1** to 11 Hz for the polyanion **1**. This can be explained due to the extreme electronegative character of the polyanion framework leading to an increase in the C-P bond distance from the free bisphosphonate ligand **L1** to the polyanion **1**. The ^{31}P NMR for polyanion **1**, shows a downfield shifted peak at 24.4 (15.8) ppm [see **Figure S9(d)** in Supporting Information] which can also be attributed to the deshielding effect of the electronegative polyanionic framework.

Unlike polyanion **1**, the ^1H NMR of polyanion **2** in the aromatic region is very difficult to assign. However, the aliphatic region shows better resolution in **2**, with respect to **1**, with the ^1H -

^{31}P coupling now clearly discernible. As per our analysis, for polyanion **2** the aromatic protons in the 2, 4, 5, and 6 position (values in parentheses for free bisphosphonate ligands) are observed at 8.94 (8.38), 8.75 (8.22), 8.41 (7.22) and 7.97 (7.79) ppm, respectively [see **Figure S10(b)** in Supporting Information]. These values clearly show that the all-aromatic protons of polyanion **2** exhibit downfield shifts of 0.558, 0.532, 1.186 and 0.183 ppm, for positions 2, 4, 5 and 6, respectively, as compared to the free bisphosphonate (**L2**), once again ostensibly due to the highly electronegative polyanionic framework. Interestingly, the proton at position 5 shows an extremely high downfield shift of 1.186 ppm. The aliphatic protons are observed as a triplet at 3.58 (3.136) ppm [see **Figure S10(c)** in Supporting Information], which shows downfield shift of 0.444 ppm. Once again, we see a decrease in the $^3J_{\text{H-P}}$ coupling constant to 11.5 Hz, from a value of 12.5 Hz in the free bisphosphonate (**L2**), which can also be attributed to the increase in the C-P bond length from the bisphosphonate to the polyanion owing to the electronegative character of the polyanion framework. Like polyanion **1**, the ^{31}P NMR for polyanion **2**, also shows a downfield shifted peak at 24.0 (17.4) ppm [see **Figure S10(d)** in Supporting Information] which can also be attributed to the deshielding effect of the electronegative polyanionic framework.

For polyanion **4**, the ^1H NMR is also well resolved in the aliphatic region only. The spectrum shows the following signals for the aromatic region (values in parentheses are for free bisphosphonate ligands) 8.29 (7.39), 8.52 (8.25) ppm, for protons at positions 2 & 6, and 3 & 5, respectively [**Figure S11(a)** and **(b)**]. These values clearly show that the all-aromatic protons of polyanion **4** exhibit downfield shifts of 0.9 and 0.27 ppm, respectively compared to the free ligand (**L3**). The aliphatic protons are observed as a triplet at 3.64 (3.156) ppm [see **Figure S11(c)** in Supporting Information], also showing a downfield shift of 0.484 ppm, corresponding to the free ligand (**L3**). Similar to polyanions **1** and **2**, a decrease in the $^3J_{\text{H-P}}$ coupling constant to 12 Hz, from

a value of 12.5 Hz in the free bisphosphonate (**L3**), is also observed for polyanion **4**. However, for polyanion **4** such a reduction in the $^3J_{\text{H-P}}$ coupling constant is less in comparison with polyanions **1** and **2**. The ^{31}P NMR for polyanion **4**, analogous to the polyanion **1** and **2**, also shows a downfield shifted peak at 23.7 (17.2) ppm [see **Figure S11(d)** in Supporting Information] which can also be attributed to the deshielding effect of the electronegative metal oxygen environment. However, the deshielding effect is observed to be more pronounced in polyanion **1** (downfield shift of 8.6 ppm), in comparison with polyanions **2** and **4** (downfield shifts of 6.6 and 6.5 ppm, respectively).

2.2.2 Optical Spectroscopy

Saturated solution of **1a** (8.8 μM), **2a** (8.4 μM), **3a** (7.6 μM), **4a** (8.2 μM) and **5a** (8.0 μM) were prepared for optical spectroscopic studies. UV-Visible spectrum for compounds **1a**, **2a**, **3a**, **4a** and **5a** were monitored in the range of 200 - 800 nm in aqueous solution. Being isostructural, polyanions **1**, **2** and **4** display close to similar optical spectra and exhibit a strong absorption peak at 263, 261 and 256 nm, respectively, in the ultra-violet region [see **Figure S12(a)**, **(b)** and **(c)**, respectively]. These strong peak(s) in the UV region can be attributed to the $p\pi-d\pi$ charge-transfer transition of the $\text{O}_t \rightarrow \text{V}$ bonds.⁴⁷ Jahn-Teller distorted transitions from $^2T_{2g} \rightarrow ^2E_g$ for V(IV) d-d transitions, are observed in the visible region. For polyanion **1** the spectra shows two less intense peaks, at 551 and 600 nm [see **Figure S12(a)** inset].⁶⁷ Similarly, polyanion **2** also shows two less intense peaks in the visible region, at 532 and 616 nm [see **Figure S12(b)** inset],⁶⁷ and polyanion **4** shows peaks at 610 and 650 nm [see **Figure S12(c)** inset].

The UV-Visible spectrum in aqueous solution of isostructural compounds **3a** and **5a** also show a characteristic peak at 254 and 263 nm, respectively, in the ultraviolet region, which can be assigned to $\text{O}_t \rightarrow \text{V}$ charge transfer transition [see **Figure S13(a)** and **(b)**, respectively].³²

Additionally, compound **5a** displays another peak in the ultraviolet region at 315 nm, corresponding to the bridging O_b→V bond [see **Figure S13(b)**]. In the visible region, polyanion **3** shows three low intense absorption peaks at 564, 609 and 636 nm, and polyanion **5** at 520, 615 and 750 nm [see **Figure S13(a)** and **(b)** inset, respectively], which can be attributed to the *z-out* type Jahn-Teller distorted ${}^2T_{2g} \rightarrow {}^2E_g$ V(IV) d-d transitions.⁶⁸

Time-dependent UV-Visible analysis confirmed compounds **1a**, **2a** and **3a** to be stable in solution for sufficient periods of time, owing to no visible change in absorbance intensity with time [Figure **S12-13**].

2.3 MAGNETIC STUDIES

Magnetic measurements were performed on polycrystalline samples of **1a**, **2a** and **3a** in the temperature range of 5-300 K, using an external dc field of 1000 Oe. Temperature dependence of χT [χ represents magnetic susceptibility per vanadium (IV) ion] for **1a**, **2a** and **3a** in cooling modes are shown (in **Figure 4**). The measured χT product for **1a** at 300 K is 0.37 cm³ mol⁻¹ K, which is in agreement with the expected value per V^{IV} ion (3d¹, $S = 1/2$, ${}^2D_{3/2}$). On lowering the temperature, the χT value remains constant down to 60 K and further lowering of temperature causes a decrease in the χT with the value reaching 0.28 cm³ mol⁻¹ K at 5 K. For **2a**, the measured χT product at 300 K is 0.39 cm³ mol⁻¹ K, which is also in agreement with the expected value per V^{IV} ion (3d¹, $S = 1/2$, ${}^2D_{3/2}$) and V^V (3d⁰). When the temperature is lowered, the χT product at 1000 Oe gradually decreases reaching 0.25 cm³ mol⁻¹ K at 5 K. For **3a**, the measured χT product is 1.08 cm³ mol⁻¹ K, which lies close to the expected value for three V^{IV} ion (3d¹, $S = 1/2$, ${}^2D_{3/2}$) ions ($\chi T = 1.05$ cm³ mol⁻¹ K for $g = 1.930$). When the temperature is lowered, the χT product at 1000 Oe remains almost constant till 50 K and then decreases down reaching 0.9 cm³ mol⁻¹ K at 5 K,

indicating weak anti-ferromagnetic interactions between the three V^{IV} atoms within the structure. It is worth to mention that the decrease in χT value at temperature below 50 K in **1a–3a** is probably due to the spin orbit coupling operational at low temperatures.

The field dependence of magnetization measurements was studied on **1a**, **2a** and **3a** from 0 – 5 T at 5, 8 and 10 K [**Figures S15, S16 and S17 (left)** for **1a**, **2a** and **3a**, respectively]. At 5 K and 5 T, the magnetization values are 0.49, 0.49 and 1.54 μ_B for **1a**, **2a** and **3a** respectively, which are slightly lower than the expected values for $S = \frac{1}{2}$ (**1a**), $S = \frac{1}{2}$ (**2a**), and three independent $S = \frac{1}{2}$ systems for (**3a**) respectively. The unsaturation character of the magnetization curve describes the lower magnetization value. Furthermore, the superimposition of M vs H/T curve onto a single master curve [**Figure S15, S16, S17 (right)** for **1a**, **2a** and **3a**, respectively] indicates the absence of magnetic anisotropy in these complexes.

Magnetic data reported for isostructural derivatives of **3a** with hydroxyethylidene-1,1-bisphosphonate,⁵⁸ and 1-hydroxy-2-(imidazole-1-yl)-1,1-bisphosphonic acid,⁵⁶ matches well with the χT values of 1.10 and 1.05 $\text{cm}^3 \text{mol}^{-1} \text{K}$ at 300K for the polyanions [$\{V_3(H_2O)O_3\}\{O_3P-C(OH)(CH_3)-PO_3\}_3\}^{5-}$,⁵⁸ [$V_3O_3(H_2O)\{O_3P-C(OH)(C_4H_6N_2)-PO_3\}_3\}^{3-}$,^{56, 58} respectively. For the polyanion [$\{V_3(H_2O)O_3\}\{O_3P-C(OH)(CH_3)-PO_3\}_3\}^{5-}$ the measured χT value was also observed to decrease down to 0.920 $\text{cm}^3 \text{mol}^{-1} \text{K}$ upon lowering the temperature to 12 K, indicating similar physical properties of **3a**. However for the polyanion [$V_3O_3(H_2O)\{O_3P-C(OH)(C_4H_6N_2)-PO_3\}_3\}^{3-}$ the χT value was observed to increase to 1.15 $\text{cm}^3 \text{mol}^{-1} \text{K}$ upon lowering the temperature down to 2 K, indicating weak ferromagnetic interactions between the V^{IV} ion for this polyanion.

2.4 ANTI-BACTERIAL STUDIES

Vanadium is an essential element in bioinorganic chemistry.⁶⁹ As such, bisphosphonate-polyoxovanadates, with their flexible assembly, potential synergistic effects of the organic moiety with the metals, and a versatile vanadium redox chemistry; are extremely interesting candidates for the study of biological activity of such compounds. Recently, artificial enzymes with oxidase and peroxidase-like activity have emerged as the intriguing alternatives of the natural enzymes with their unique properties.⁷⁰⁻⁷² Peroxidase-like artificial enzyme were used to enhance the bactericidal ability of the traditional disinfectant agent; H₂O₂ solution.⁷³⁻⁷⁴ Conventional use of the higher concentration of H₂O₂ restrain its various application because of its potential side effects, such as harsh bleaching effect, corrosion etc.⁷⁵⁻⁷⁷ Artificial enzymes with peroxidase-like activity can catalyze the decomposition of H₂O₂ into ·OH radical, that generate very high oxidative stress under milder condition. The high oxidative stress at low concentration of H₂O₂ impairs the bacterial cell membrane integrity to show elevated bactericidal effect.⁷⁸⁻⁷⁹ Furthermore, it has been reported that nanosized V₂O₅ can exhibit glutathione peroxidase (GPx)-like activity and CeVO₄ superoxide dismutase like activity.⁸⁰⁻⁸¹

In order to explore the anti-bacterial properties of our synthesized bisphosphonate-polyoxovanadates, we explored the peroxidase-like activity of these compounds, that catalyze the decomposition of H₂O₂ into [[·]OH] radical at benign condition. The compounds are observed to exhibit very high antibacterial activity against methicillin-resistant *staphylococcus aureus* (MRSA) bacterial strain. Several reports are present in the literature of anti-bacterial studies with polyoxometalates,⁸²⁻⁸⁴ however, none so with bisphosphonate-polyoxometalate compounds. We have been able to quantitatively assess the anti-bacterial activity of compounds **1a** and **2a** only, owing to the extremely low solubility of compound **3a**.

2.4.1 Estimation of Peroxidase-like Activity.

The peroxidase activity of the compounds **1a** and **2a** were determined using colorimetric method, wherein 3,3',5,5'-tetramethylbenzidine (TMB) was used as a substrate, that upon oxidation showed a distinct color change. The activity was monitored by measuring absorbance at 652 nm. From **figure 5**, in presence of both the compounds **1a** and **2a** significant activity was obtained in acetate buffer medium (pH 4.2). In contrary with only H₂O₂ as a control, there was no such activity observed. This clearly indicates the catalytic activity of the compounds. The dose-dependent activity assays were performed in presence of H₂O₂ (2.5 mM) with various concentration of the compounds ranging from 20 to 100 µg/mL [see **Figure S18** in Supporting Information]. The activity was observed to increase with increasing concentrations of the compounds.

The kinetic study for the peroxidase-like activity of the compounds **1a** and **2a** were performed to estimate the Michaelis-Menten constant (K_m) that represents the affinity of the substrate molecules to the enzyme [see **Figure S19** in Supporting Information]. The smaller K_m value indicates higher affinity and vice versa. The K_m values for the compounds **1a** and **2a** were obtained as 0.0243 mM and 0.0279 mM, respectively, which is comparable to many other reported systems.

2.4.2 Hydroxy Radical [\bullet OH] Detection Assay.

To evaluate the mechanism for the catalytic decomposition of H₂O₂ in presence of the peroxidase-like bisphosphonate-polyoxovanadate compounds, we have performed terephthalic acid (TA) assay, where terephthalic acid was used as a fluorescence probe. Oxidation of terephthalic acid with [\bullet OH] radical is a selective reaction and gives 2-hydroxy terephthalic acid (TAOH) that shows a specific fluorescence emission peak at 435 nm. In case of the assay (TA + vanadate compound + H₂O₂), the observance of fluorescence peak with enhanced intensity compared to the other

composition assays suggested the generation of [\bullet OH] radical from the catalytic decomposition of H_2O_2 .

2.4.3 Artificial Enzyme Assisted Enhanced Antibacterial Activity of H_2O_2 .

The estimation of the enhanced antibacterial activity of H_2O_2 in presence of compounds **1a** and **2a** were performed using a pathogenic bacteria MRSA. The peroxidase-like activity of the compounds catalyzed the decomposition of H_2O_2 to reactive [\bullet OH] radicals, that generates very high oxidative stress. Thus, it can impair the cell membrane integrity, causing the bactericidal effect. The plate count method was used to determine the antibacterial activity. In **figure 7**, the result revealed that the bacterial survival ability conspicuously reduced up to 99.9% in presence compound **2a** and complete reduction happened for compound **1a** along with only 0.5 mM H_2O_2 , whereas H_2O_2 alone was not able to inhibit the bacterial growth. This manifested the amplification of antibacterial activity of H_2O_2 in presence of the polyoxovanadate compounds. Moreover, only the vanadate compounds showed no antibacterial activity [see **Figure S20** in Supporting Information] which implies that the overall complex plays the crucial role in enzymatic and antibacterial activity.

3. EXPERIMENTAL

MATERIALS AND METHODS

Vanadium compounds {V₂O₅ from Merck-Sigma-Aldrich (>98%), VOSO₄ from Alfa Aesar (99.9%)}, precursors used for bisphosphonate synthesis (2, 3, 4-Pyridylacetic acid hydrochloride from Merck-Sigma-Aldrich with 99% purity), 3,3',5,5'-Tetramethylbenzidine (TMB), terephthalic acid and H₂O₂ (30%) were obtained from commercial sources.

PXRD data was collected on Bruker D8ECO with Cu-K α source radiation ($\lambda = 1.54056 \text{ \AA}$) from angular range 5 to 50 ° at 298 K. The Infrared spectra were recorded on ThermoFisher Scientific iS50 spectrometer (4000 – 400 cm⁻¹). Thermogravimetric analysis (TG/DTA) was performed on thermal analyzer TG-DTA7200 (HITACHI, Japan) over a temperature range of 40 to 900 °C at a heating rate of 10 °C min⁻¹ under the nitrogen gas atmosphere. Elemental analysis for C, H, N and O was performed on Thermo Scientific Flash 2000 Organic Elemental Analyzer (CHNS/O Mode). Elemental analysis for V and P was performed using ICP-AES method with **xxxx**

NMR spectra was measured with Varian Inova 500 MHz. UV-Visible was conducted on JASCO UV (V-630) in the range of 200-800 nm. For the time-dependent UV-Visible spectra, the aqueous solution of the compounds were kept standing in the cuvette and spectra measured at period time-intervals.

The peroxidase-like activity assay was performed with a ThermoFisher Scientific plate reader and Milli-Q water was used throughout our study.

Magnetism data for **1a–3a** was collected on a Quantum Design MPMS–XL EverCool SQUID Magnetometer in temperature ranging from 5 – 300 K, under an applied external dc field in the range of –5 T to 5 T. Polycrystalline sample of **1a–3a**, (17.12, 14.20 and 13.28 mg, respectively), sealed inside polypropylene bag (2.8 × 0.75 × 0.02 cm) were subjected to measurement. *M vs H*

data was recorded for all three at 100 K to check for the presence of any ferromagnetic impurity which was found to be absent. Magnetization as a function of temperature was measured under 1000 Oe external dc field. The isothermal magnetization was studied at 5, 8, and 10 K. The magnetic data was corrected for the sample holder and the diamagnetic contribution.

Single-Crystal X-ray Diffraction. Single crystals of **1a**, **2a** and **3a** were mounted on a Hampton on a BRUKER AXS (D8 Quest System) X-ray diffractometer equipped with PHOTON 100 CMOS detector using Mo K α radiation ($\lambda = 0.71073 \text{ \AA}$), at 293(2) K. Direct methods were used to solve the structures and to locate the heavy atoms (SHELXS97), and the remaining atoms were found from successive difference maps (SHELXL97).⁸⁵ Routine Lorentz and polarization corrections were applied, and an absorption correction was performed using the SADABS program.⁸⁶ For **1a**, **2a** and **3a** the hydrogens of all the C, O and N atoms were added in calculated positions and refined using a riding model. Crystallographic data are summarized in Table 1.

Synthesis: Bisphosphonic acid precursors. The bisphosphonic acid precursors, **L1**, **L2**, **L3**, were synthesized according to literature⁸⁷ and characterized using NMR spectroscopy. **L1** ¹H NMR (500 MHz, D₂O/NH₃): δ (ppm) 3.567 (t, ³J_{H-P} = 12.5 Hz, 2H), 7.785 (t, ²J_{H-H} = 7 Hz, 1H), 7.897 (d, ²J_{H-H} = 8 Hz, 1H), 8.350 (t, ²J_{H-H} = 8 Hz, 1H), 8.522 (d, ²J_{H-H} = 5.5 Hz, 1H). ³¹P NMR (500 MHz, D₂O/NH₃): δ (ppm) 15.8. **L2** ¹H NMR (500 MHz, D₂O/NH₃): δ (ppm) 3.136 (t, ³J_{H-P} = 12.5 Hz, 2H), 7.224 (dt, ²J_{H-H} = 5 and 8 Hz, 1H), 7.791 (dt, ²J_{H-H} = 1.5 and 8 Hz, 1H), 8.218 (dd, ²J_{H-H} = 1.5 and 5 Hz, 1H), 8.382 (d, ²J_{H-H} = 2 Hz, 1H). ³¹P NMR (500 MHz, D₂O/NH₃): δ (ppm) 17.4. **L3** ¹H NMR (500 MHz, D₂O/NH₃): δ (ppm) 3.156 (t, ³J_{H-P} = 12.5 Hz, 2H), 7.391 (d, ²J_{H-H} = 6 Hz, 2H), 8.259 (d, ²J_{H-H} = 6 Hz, 2H). ³¹P NMR (500 MHz, D₂O/NH₃): δ (ppm) 17.2.

*(NH₄)₄[H₆(V^{IV}O₂)(V^V₂O₅)₂{O₃P-C(O)(CH₂-2-C₅NH₄)-PO₃}₂] \cdot 9H₂O (**1a**):* In a typical synthesis, to 10 ml of 2M ammonium acetate buffer (pH 4.7) V₂O₅ (0.1003 g, 0.5 mmol) and 1-hydroxy-2-(2-

pyridyl) ethylidene-1,1-bisphosphonic acid (**L1**) (0.1390 g, 0.5 mmol) were added. The solution was stirred for a further 30 minutes at 80 °C and left to evaporate at room temperature. Green colored crystals were collected after 20 days. Yield: 0.1021 g (20 % based on V). Elemental analysis (%) Calcd. for **1a**: V, 20.49; P, 9.97; C, 13.53; H, 4.22; N, 6.76; O, 45.04. Found: V, 20.27; P, 9.85; C, 13.83; H, 3.72; N, 6.65; O, 45.56. ¹H NMR (500 MHz, D₂O): δ (ppm) 3.774 (t, ³J_{H-P} = 11 Hz, 2H), 7.72 (1H), 8.26 (1H), 8.424 (1H), 8.60 (1H). ³¹P NMR (500 MHz, D₂O): δ (ppm) 24.4. Thermogravimetric analysis shows a weight loss of approximate 13% for crystal water from compound **1a** (Figure S22).

$(NH_4)_4[H_6(V^{IV}O_2)(V^V_2O_5)_2\{O_3P-C(O)(CH_2-3-C_5NH_4)-PO_3\}_2]\cdot 8H_2O$ (**2a**): The synthesis of **2a** was identical with respect to **1a**, except for the use of **L2** instead of **L1**. V₂O₅ (0.1003 g, 0.5 mmol) and 1-hydroxy-2-(3-pyridyl) ethylidene-1,1-bisphosphonic acid (**L2**) (0.1390 g, 0.5 mmol) were added to 10 ml of 2M ammonium acetate buffer (pH 4.7) solution. The solution was stirred for a further 30 minutes at 80°C and left to evaporate at room temperature. Green colored crystals were collected after 6 days. Yield: 0.1526 g (50 % based on V). Elemental analysis (%) Calcd. for **2a**: V, 20.79; P, 10.11; C, 13.72; H, 4.11; N, 6.86; O, 44.40. Found: V, 20.61; P, 9.90; C, 13.66; H, 3.48; N, 6.34; O, 44.50. ¹H NMR (500 MHz, D₂O): δ (ppm) 3.58 (t, ³J_{H-P} = 11.5 Hz, 2H), 7.974 (1H), 8.41 (1H), 8.75 (1H), 8.94 (1H). ³¹P NMR (500 MHz, D₂O): δ (ppm) 24.0. Thermogravimetric analysis shows a weight loss of approximate 11.5% for crystal water from compound **2a** (Figure S22).

$(NH_4)_2[H_6(V^{IV}O)_3(O)\{O_3P-C(OH)(CH_2-4-C_5NH_4)-PO_3\}_3]\cdot 26H_2O$ (**3a**): VOSO₄ (0.0889 g, 0.5 mmol), 1-hydroxy-2-(4-pyridyl) ethylidene-1,1-bisphosphonic acid (0.1390 g, 0.5 mmol) (**L3**) and pyrazine (0.0402 g, 0.5 mmol) were added to 10 ml of 2M ammonium acetate buffer (pH 4.7) solution. The solution was stirred for a further 15 minutes at 60 °C and left to evaporate at room

temperature. Green colored crystals were collected after 2 days. Yield: 0.1350 g (20.40 % based on V). Elemental analysis (%) Calcd. for **3a**: V, 9.77; P, 11.88; C, 16.12; H, 5.60; N, 4.48; O, 52.15. Found: V 9.60, P 11.72, C, 16.96; H, 5.09; N, 5.13; O, 50.17. Thermogravimetric analysis shows a weight loss of approximate 21% for crystal water from compound **3a** (Figure S22).

$(NH_4)_4[H_6(V^{IV}O_2)(V^{V}_2O_5)_2\{O_3P-C(O)(CH_2-4-C_5NH_4)-PO_3\}_2]\cdot 11H_2O$ (**4a**): The synthesis of **4a** was identical with respect to **1a**, except for the use of **L3** instead of **L1**. V_2O_5 (0.1003 g, 0.5 mmol) and 1-hydroxy-2-(4-pyridyl) ethylidene-1,1-bisphosphonic acid (**L3**) (0.1390 g, 0.5 mmol) were added to 10 ml of 2M ammonium acetate buffer (pH 4.7) solution. The solution was stirred for a further 30 minutes at 80°C and left to evaporate at room temperature. Green colored powder was collected after 6 days. Yield: 0.1005 g (20 % based on V). Elemental analysis (%) Calcd. for **4a**: V, 19.91; P, 9.69; C, 13.14; H, 4.41; N, 6.57; O, 46.28. Found: V, 19.1; P, 8.92; C, 14.42; H, 5.08; N, 7.16; O, 47.52. 1H NMR (400 MHz, D_2O): δ (ppm) 3.64 (t, $^3J_{H-P} = 12$ Hz, 2H), 8.29 (2H), 8.52 (2H). ^{31}P NMR (400 MHz, D_2O): δ (ppm) 23.7. Thermogravimetric analysis shows a weight loss of approximate 17% for crystal water from compound **4a** (Figure S22).

$(NH_4)_2[H_6(V^{IV}O)_3(O)\{O_3P-C(OH)(CH_2-3-C_5NH_4)-PO_3\}_3]\cdot 21H_2O$ (**5a**): The synthesis of **4a** was identical with respect to **3a**, except for the use of **L2** instead of **L3**. $VOSO_4$ (0.0889 g, 0.5 mmol), 1-hydroxy-2-(3-pyridyl) ethylidene-1,1-bisphosphonic acid (0.1390 g, 0.5 mmol) (**L2**) and pyrazine (0.0402 g, 0.5 mmol) were added to 10 ml of 2M ammonium acetate buffer (pH 4.7) solution. The solution was stirred for a further 15 minutes at 60 °C and left to evaporate at room temperature. Green colored powder was collected after 2 days. Yield: 0.0791 g (8.8 % based on V). Elemental analysis (%) Calcd. for **5a**: V, 10.36; P, 12.60; C, 17.11; H, 5.26; N, 4.75; O, 49.91. Found: V, 9.84; P, 11.51; C, 17.55; H, 5.95; N, 4.93; O, 51.1. Thermogravimetric analysis shows a weight loss of approximate 28.2% for crystal water from compound **5a** (Figure S22).

Peroxidase-like Activity Assay. Peroxidase-like catalytic activity were estimated using colorimetric assays, where TMB was used as a substrate molecule. The progress of the reaction was monitored by measuring the absorbance of oxidized TMB at 652 nm using a plate reader. Different compounds (50 $\mu\text{g/mL}$) and TMB (0.5 mM) were added into a 96-well plate containing acetate buffer (0.1 M, pH = 4.2), then H_2O_2 (2.5 mM) solution was added and the plate was placed inside the plate reader. The values of the kinetic parameters were obtained by analyzing the kinetic plot using Michaelis-Menten equation, $v = v_{\text{max}} \times [\text{S}] / (\text{K}_m + [\text{S}])$, where v is the initial reaction velocity, $[\text{S}]$ is the substrate concentration and v_{max} is the maximal velocity.

Assay for the Detection of Hydroxy Radical. Terephthalic acid (TA) assay was used to detect the formation of hydroxyl radical.⁸⁸ The $[\bullet\text{OH}]$ radical react with terephthalic acid to form 2-hydroxy terephthalic acid, that showed a fluorescence peak at 435 nm upon excitation at 315 nm. In detail, a series of solutions with TA (0.5 mM), H_2O_2 (5 mM) and the compounds **1a** or **2a** (100 $\mu\text{g/mL}$) were mixed in acetate buffer (0.1 M, pH = 4.2). The final solutions were kept at 37 °C under dark for 6 h, then their fluorescence emissions were analyzed. All the concentrations mentioned above were the final concentrations.

Antibacterial Activity. The antibacterial activities were carried out against MRSA bacteria using a plate counting method. In short, the bacteria solution was cultured up to the mid phase growth, then the bacteria solution was centrifuged, washed and redispersed in phosphate buffer saline (PBS, 10 mM, pH = 7.4). The bacterial solution was further diluted to adjust the final optical density, $A_{600} = 0.01$ ($10^6 - 10^7$ bacteria per ml). Then the several aliquots of the bacterial solution were inoculated with H_2O_2 (0.5 mM) and the compounds **1a** or **2a** (50 $\mu\text{g/mL}$) in acetate buffer medium (0.1 M, pH = 4.2). Finally, it was incubated at 37 °C for 2h, then a small portion of each solution was uniformly dispersed on nutrient agar plate.

In vitro antibacterial activity. The in vitro antibacterial activity was performed in acetate buffer medium of pH 4.2 as a primary medium. After the secondary culture of MRSA bacteria in LB medium, the bacteria were collected by centrifugation and dispersed in PBS buffer. This we have used as bacterial stock solution. From this main bacterial stock solution only a small amount of bacterial solution (around 10 μ L in 200 μ L of acetate buffer to maintain the final OD=0.01) was transferred to the final reaction medium of acetate buffer containing the compounds and H₂O₂ solutions. There was no significant change observed in the pH of the final acetate buffer reaction medium. Hence, the pH of the final reaction mixture remains 4.2.

4. CONCLUSIONS

We have successfully synthesized five new bisphosphonate-polyoxovanadate compounds,



by the one-pot reactions of vanadium containing oxo compounds with 1-hydroxy-2-(2-pyridyl) ethylidene-1,1-bisphosphonic acid (**L1**), 1-hydroxy-2-(3-pyridyl) ethylidene-1,1-bisphosphonic acid (**L2**), 1-hydroxy-2-(4-pyridyl) ethylidene-1,1-bisphosphonic acid (**L3**), respectively, in ammonium acetate buffer solution (pH 4.7). Formation of an isostructural derivative of **1a** & **2a** with **L3**, compound **4a**; and of **3a** with **L2**, compound **5a**, respectively; were confirmed with thorough infrared spectroscopic studies of the products obtained. Polyanions $[(\text{V}^{\text{IV}}\text{O}_2)(\text{V}^{\text{V}}_2\text{O}_5)_2\{\text{O}_3\text{P-C(O)}(\text{CH}_2\text{-2-C}_5\text{NH}_4\text{-PO}_3\}_2)]^{10-}$ (**1**), $[(\text{V}^{\text{IV}}\text{O}_2)(\text{V}^{\text{V}}_2\text{O}_5)_2\{\text{O}_3\text{P-C(O)}(\text{CH}_2\text{-3-C}_5\text{NH}_4\text{-PO}_3\}_2)]^{10-}$ (**2**) and $[(\text{V}^{\text{IV}}\text{O}_2)(\text{V}^{\text{V}}_2\text{O}_5)_2\{\text{O}_3\text{P-C(O)}(\text{CH}_2\text{-4-C}_5\text{NH}_4\text{-PO}_3\}_2)]^{10-}$ (**4**) are a mixed-valent V(IV-V) assembly having a S-shaped structure of a centrally located $\{\text{V}^{\text{IV}}\text{O}_2\}$ connected alternatively with two dimeric $\{\text{V}^{\text{V}}_2\text{O}_5\}$ units by two bisphosphonate groups. Polyanions $[(\text{V}^{\text{IV}}\text{O})_3(\text{O})\{\text{O}_3\text{P-C(OH)}(\text{CH}_2\text{-4-C}_5\text{NH}_4\text{-PO}_3\}_3)]^{8-}$ (**3**) and $[(\text{V}^{\text{IV}}\text{O})_3(\text{O})\{\text{O}_3\text{P-C(OH)}(\text{CH}_2\text{-3-C}_5\text{NH}_4\text{-PO}_3\}_3)]^{8-}$ (**5**) form a triangular assembly of three units connected by three bisphosphonate groups, alternatively, and having a centrally located oxygen-atom upon a 3-fold axis of symmetry for polyanion **3**. Packing arrangement of compounds **1a**, **2a** and **3a** are observed to be influence by significant non-bonding interactions. Owing to its extremely symmetric structure as well as arrangement along three-dimensions in the crystal, compound **3a** is observed to contain significant voids in between the

molecules, in the solid-state. NMR spectroscopic studies of **1a**, **2a** and **4a** show downfield and upfield shift(s) of the aromatic proton(s), and the expected downfield shift(s) of the aliphatic proton(s) and the phosphorous nuclei. A decrease in the $^3J_{\text{H-P}}$ coupling constant(s) for the aliphatic protons coupling with phosphorous nuclei (from free ligand to the polyanion) is indicative of the electronegative nature of the polyanion framework thereby resulting in an increase of P-C bond-length due to complex formation. Additional solution phase studies, using optical spectroscopy and multi-nuclear NMR spectroscopy, indicate the prolonged stability of the polyanion structures in solution. Further solid-state characterization of the compounds using magnetism measurements reveals χT values expected for isolated V^{IV} ion ($3d^1$, $S = 1/2$, $^2D_{3/2}$) in compounds **1a**, **2a** and **3a**. However, for the compound **3a** the χT product of $1.08 \text{ cm}^3 \text{ mol}^{-1} \text{ K}$ is slightly higher than the expected value per V^{IV} ion ($3d^1$, $S = 1/2$, $^2D_{3/2}$) and V^{V} ($3d^0$). The synthesized compounds **1a** and **2a** show significant anti-bacterial properties with respect to peroxidase-like activity, which is attributed to the enhancement of the antibacterial activity in the presence of H_2O_2 . With such investigations, we can conclude that the artificial enzyme potentiated amplified antibacterial activity of H_2O_2 of such hybrid compounds would be an extremely effective tool to combat with the spread of infectious diseases.

Table 1. Crystal Data and Structure Refinement Parameters for compounds **1a**, **2a**, and **3a**

Compound	1a	2a	3a
Empirical formula	V ₅ P ₄ O ₃₅ C ₁₄ N ₆ H ₅₂	V ₅ P ₄ O ₃₄ C ₁₄ N ₆ H ₅₀	V ₃ P ₆ C ₂₁ O ₅₁ N ₅ H ₈₇
Molar mass (g mol ⁻¹)	1243.19	1225.18	1564.59
Crystal System	Orthorhombic	Orthorhombic	Trigonal
Space Group	<i>P2₁2₁2</i>	<i>P2₁2₁2</i>	<i>R$\bar{3}$c</i>
a (Å)	14.973(4)	14.943(3)	18.076(4)
b (Å)	30.151(9)	30.701(6)	18.076(4)
c (Å)	9.472(3)	9.554(2)	67.226(15)
α (°)	90	90	90
β (°)	90	90	90
γ (°)	90	90	120
Volume (Å ³)	4276(2)	4383.0(14)	19023(7)
Z	2	2	6
Temp (K)	298	298	298
F _{calcd} (g cm ⁻³)	1.931	1.857	1.639
Abs coeff	1.318	1.283	0.701
GoF	1.077	1.096	1.057
R1 ^a [I > 2 σ (I)]	0.0492	0.0807	0.0975
wR2 ^a	0.1371	0.1894	0.1965

^a R1 = $\Sigma||F_o| - |F_c||/\Sigma|F_o|$. wR2 = $\{\Sigma[w(F_o^2 - F_c^2)]/\Sigma[w(F_o^2)^2]\}s^{1/2}$.

Table 2. Comparison between the mixed-valent polyoxovanadate open structures with bisphosphonate ligands

Sl. No.	Formula	Bisphosphonate ligand	Structure	Range of V-O bond distances (Å)	Crystal symmetry	Reference
1.	$[(V^{IV}O_2)(V^{V}_2O_5)_2\{O_3P-C(O)(C_3H_6NH_3)-PO_3\}_2]^{4-}$	4-amino-1-hydroxybutane-1,1-bisphosphonate	U-shaped	1.590 – 2.290	$Pna2_1$	56
2.	$[(V^{IV}O_2)(V^{V}_2O_5)_2\{O_3P-C(O)(C_4H_6N_2)-PO_3\}_2]^{4-}$	1-hydroxy-2-(imidazole-1-yl)ethane-1,1-bisphosphonate	S-shaped	1.575 – 2.348	$P2_12_12$	56
3.	$[(V^{IV}O_2)(V^{V}_2O_5)_2\{O_3P-C(O)(CH_2-2-C_5NH_4)-PO_3\}]^{10-}$	1-hydroxy-(2-pyridyl)ethane-1,1-bisphosphonate	S-shaped	1.5840 – 2.3631	$P2_12_12$	This Article
4.	$[(V^{IV}O_2)(V^{V}_2O_5)_2\{O_3P-C(O)(CH_2-3-C_5NH_4)-PO_3\}_2]^{10-}$	1-hydroxy-(3-pyridyl)ethane-1,1-bisphosphonate	S-shaped	1.5672 – 2.3860	$P2_12_12$	This Article

Table 3. Comparison between the polyoxovanadate(IV) trimeric structures with bisphosphonate ligands

Sl. No.	Formula	Bisphosphonate ligand	Structure	Range of V-O bond distances (Å)	Crystal symmetry	Reference
1.	$[(V^{IV}O)_3\{O_3P-C(OH)(CH_3)-PO_3\}_3]^{5-}$	1-hydroxyethane-1,1-bisphosphonate	Triangular	1.514 – 2.289 1.504 – 2.71	$P-1$ $P6_3/m$	58 57
2.	$[(V^{IV}O)_3\{O_3P-C(OH)(C_4H_6N_2)-PO_3\}_3]^{3-}$	1-hydroxy-2-(imidazole-1-yl)ethane-1,1-bisphosphonate	Triangular	1.628 – 2.881	$P2_1/c$	56
3.	$[(V^{IV}O)_3\{O_3P-C(OH)(C_3H_6NH_3)-PO_3\}_3]^{3-}$	4-amino-1-hydroxybutane-1,1-bisphosphonate	Triangular	1.634 – 2.242	$P-1$	60
4.	$[(V^{IV}O)_3(O)\{O_3P-C(OH)(CH_2-4-C_5NH_4)-PO_3\}_3]^{8-}$	1-hydroxy-(4-pyridyl)ethane-1,1-bisphosphonate	Triangular	1.7939 – 2.4457	$R\bar{3}c$	This Article

ASSOCIATED CONTENT

Supporting Information

Table S1-S3: Bond-valence sum calculations for polyanions **1**, **2** and **3**, respectively.

Table S4-S6: Hydrogen-bonding parameters for compounds **1a**, **2a** and **3a**, respectively.

Figure S1-S3. Comparative powder-XRD pattern(s) of compounds **1a**, **2a** and **3a**, respectively.

Figure S4. Comparative IR spectrum for compounds **1a**, **2a** and **4a**.

Figure S5. Comparative IR spectrum for products obtained upon reaction of VO_2SO_4 with **L1** and compounds **5a** and **3a**.

Figure S6. Solid-state arrangement of compound **1a**: (a) One-dimensional chain of **1a** arranged in the solid-state running parallel along a-axis. (b) Packing of compound **1a** in the solid state showing the π - π staking between the aromatic rings of neighbouring polyanions.

Figure S7 Solid-state arrangement of compound **2a**: (a) One-dimensional chain of **2a** arranged in the solid-state running parallel along a-axis. (b) Packing of compound **2a** in the solid state showing the π - π staking between the aromatic rings of neighbouring polyanions.

Figure S8. Solid-state arrangement of compound **3a**: Packing of **3a** in the solid state forming hexagonal arrangement around one polyanion unit.

Figure S9-S11. Representative NMR Spectra of polyanion(s) **1**, **2** and **4**, respectively, (a) complete ^1H NMR spectra, (b) aromatic region, (c) aliphatic region, (d) ^{31}P NMR spectra.

Figure S12. UV-Visible spectrum for compound (a) **1a**, (b) **2a**, and (c) **4a**, respectively. Inset shows the visible region.

Figure S13. UV-Visible spectrum for compound (a) **3a**, (b) **5a**. Inset shows the visible region.

Figure S14. Field dependence of the magnetization plotted as M vs H for **1a** (top), **2a** (middle) and **3a** (bottom) at 100 K. The solid lines represent the best fit.

Figure S15-S17. Field dependence of the magnetization plotted as M vs H (left) and M vs H/T (right) plots for **1a-3a** at 5, 8 and 10 K. The solid lines are guide for the eyes.

Figure S18. (a) Dose dependent activity of the compound **1a** (20-100 $\mu\text{g/mL}$) and **(b)** compound **2a** (20-100 $\mu\text{g/mL}$) in presence of TMB (0.5 mM) and H_2O_2 (2.5 mM) in acetate buffer medium.

Figure S19. (a) Kinetic plot of the compound **1a** (50 $\mu\text{g/mL}$) and **(b)** compound **2a** (50 $\mu\text{g/mL}$) in presence of TMB (0.5 mM) and H_2O_2 (0.025 -2.5 mM) in acetate buffer medium.

Figure S20. Photographs of MRSA bacterial colonies formed after exposure to the **(a)** compound **1a** (50 $\mu\text{g/mL}$) and **(b)** compound **2a** (50 $\mu\text{g/mL}$) for 2h.

Figure S21. The reaction schemes for (a) the peroxidase-like catalytic activity of the polyoxovanadate anions, and (b) reaction between hydroxyl radical ($\bullet\text{OH}$) and terephthalic acid (TA).

Figure S22. Comparative TGA graph for compound **1a, 2a, 3a, 4a** and **5a**.

Accession Codes

CCDC 2018570, 2018571, 2018572 contain the supplementary crystallographic data for this paper. These data can be obtained free of charge via www.ccdc.cam.ac.uk/data_request/cif, or by emailing data_request@ccdc.cam.ac.uk, or by contacting The Cambridge Crystallographic Data Centre, 12 Union Road, Cambridge CB2 1EZ, UK; fax: +44 1223 336033.

AUTHOR INFORMATION

Corresponding Author

*Abhishek Banerjee – Department of Chemistry, Visvesvaraya National Institute of Technology, Nagpur, India; <https://orcid.org/0000-0003-4552-4820>;

E-mail: abhishekbannerjee@chm.vnit.ac.in

*Debajit Sarma – Department of Chemistry, Indian Institute of Technology Patna, Patna, India;

<https://orcid.org/0000-0002-9830-4808>; E-mail: debajit@iitp.ac.in

ACKNOWLEDGMENT

DT Thanks VNIT, Nagpur for providing doctoral fellowship. NA thanks IIT Patna for providing doctoral fellowship. AB thanks SERB (Grant No. ECR/2017/000932) and CSIR (Grant No. 01(3004)/19/EMR-II) for financial assistance. AM thanks the Indian Institute of Science (IISc) Bangalore, India, and the Indo-Russia Joint Research Funding, Project No: INT/RUS/RFBR/373) for financial support. MD thanks SERB (CVD/2020/000855) for financial support. The authors are grateful to DST-FIST (SR/FIST/CSI-279/2016(C)) for providing characterization facility. The authors thank SAIF IIT Patna for Single crystal X-ray diffraction facility.

REFERENCES

1. Pope, M. T.; Müller, A., Introduction to Polyoxometalate Chemistry : From Topology via Self-assembly to Applications. In *Polyoxometalate Chemistry From Topology via Self-Assembly to Applications*, Pope, M. T.; Müller, A., Eds. Springer Netherlands: Dordrecht, 2001; pp 1-6.
2. Kortz, U.; Müller, A.; van Slageren, J.; Schnack, J.; Dalal, N. S.; Dressel, M., Polyoxometalates: Fascinating structures, unique magnetic properties, *Coord. Chem. Rev.* **2009**, 253 (19), 2315-2327.
3. Ishizuka, T.; Ohkawa, S.; Ochiai, H.; Hashimoto, M.; Ohkubo, K.; Kotani, H.; Sadakane, M.; Fukuzumi, S.; Kojima, T., A supramolecular photocatalyst composed of a polyoxometalate and a photosensitizing water-soluble porphyrin diacid for the oxidation of organic substrates in water, *Green Chem.* **2018**, 20 (9), 1975-1980.
4. Zhang, Z.; Zhu, Q.; Sadakane, M.; Murayama, T.; Hiyoshi, N.; Yamamoto, A.; Hata, S.; Yoshida, H.; Ishikawa, S.; Hara, M.; Ueda, W., A zeolitic vanadotungstate family with structural diversity and ultrahigh porosity for catalysis, *Nat. Commun.* **2018**, 9 (1), 3789.
5. Pope, M. T., Heteropoly and Isopoly Oxometalates, *Springer-Verlag* **1983**.
6. Moussawi, M. A.; Haouas, M.; Floquet, S.; Shepard, W. E.; Abramov, P. A.; Sokolov, M. N.; Fedin, V. P.; Cordier, S.; Ponchel, A.; Monflier, E.; Marrot, J.; Cadot, E., Nonconventional Three-Component Hierarchical Host–Guest Assembly Based on Mo-Blue Ring-Shaped Giant Anion, γ -Cyclodextrin, and Dawson-type Polyoxometalate, *J. Am. Chem. Soc.* **2017**, 139 (41), 14376-14379.
7. Oms, O.; Dolbecq, A.; Mialane, P., Diversity in structures and properties of 3d-incorporating polyoxotungstates, *Chem. Soc. Rev.* **2012**, 41 (22), 7497-7536.

8. Rom, T.; Paul, A. K., Role of aromatic vs. aliphatic amine for the variation of structural, electrical and catalytic behaviors in a series of silver phosphonate extended hybrid solids, *Dalton Trans.* **2020**, *49* (39), 13618-13634.
9. Paul, A. K.; Kanagaraj, R.; Jana, A. K.; Maji, P. K., Novel amine templated three-dimensional zinc-organophosphonates with variable pore-openings, *Cryst. Eng. Comm.* **2017**, *19* (43), 6425-6435.
10. Banerjee, A.; Bassil, B. S.; Röschenhaler, G.-V.; Kortz, U., Diphosphates and diphosphonates in polyoxometalate chemistry, *Chem. Soc. Rev.* **2012**, *41* (22), 7590-7604.
11. Dolbecq, A.; Mialane, P.; Sécheresse, F.; Keita, B.; Nadjo, L., Functionalized polyoxometalates with covalently linked bisphosphonate, N-donor or carboxylate ligands: from electrocatalytic to optical properties, *Chem. Commun.* **2012**, *48* (67), 8299-8316.
12. Singh, A. P.; Zhang, Y.; No, J.-H.; Docampo, R.; Nussenzweig, V.; Oldfield, E., Lipophilic Bisphosphonates Are Potent Inhibitors of Plasmodium Liver-Stage Growth, *Antimicrob. Agents Chemother.* **2010**, *54* (7), 2987.
13. Mukherjee, S.; Huang, C.; Guerra, F.; Wang, K.; Oldfield, E., Thermodynamics of Bisphosphonates Binding to Human Bone: A Two-Site Model, *J. Am. Chem. Soc.* **2009**, *131* (24), 8374-8375.
14. Zhang, Y.; Hudock, M. P.; Krysiak, K.; Cao, R.; Bergan, K.; Yin, F.; Leon, A.; Oldfield, E., Activity of Sulfonium Bisphosphonates on Tumor Cell Lines, *J. Med. Chem.* **2007**, *50* (24), 6067-6079.
15. Clézardin, P., Bisphosphonates' antitumor activity: An unravelled side of a multifaceted drug class, *Bone* **2011**, *48* (1), 71-79.

16. Bivi, N.; Bereszczak, J. Z.; Romanello, M.; Zeef, L. A. H.; Delneri, D.; Quadrifoglio, F.; Moro, L.; Brancia, F. L.; Tell, G., Transcriptome and Proteome Analysis of Osteocytes Treated with Nitrogen-Containing Bisphosphonates, *J. Proteome Res.* **2009**, *8* (3), 1131-1142.
17. Martin, M. B.; Sanders, J. M.; Kendrick, H.; de Luca-Fradley, K.; Lewis, J. C.; Grimley, J. S.; Van Brussel, E. M.; Olsen, J. R.; Meints, G. A.; Burzynska, A.; Kafarski, P.; Croft, S. L.; Oldfield, E., Activity of Bisphosphonates against *Trypanosoma brucei rhodesiense*, *J. Med. Chem.* **2002**, *45* (14), 2904-2914.
18. Zhang, Y.; Leon, A.; Song, Y.; Studer, D.; Haase, C.; Koscielski, L. A.; Oldfield, E., Activity of Nitrogen-Containing and Non-Nitrogen-Containing Bisphosphonates on Tumor Cell Lines, *J. Med. Chem.* **2006**, *49* (19), 5804-5814.
19. Martin, M. B.; Grimley, J. S.; Lewis, J. C.; Heath, H. T.; Bailey, B. N.; Kendrick, H.; Yardley, V.; Caldera, A.; Lira, R.; Urbina, J. A.; Moreno, S. N. J.; Docampo, R.; Croft, S. L.; Oldfield, E., Bisphosphonates Inhibit the Growth of *Trypanosoma brucei*, *Trypanosoma cruzi*, *Leishmania donovani*, *Toxoplasma gondii*, and *Plasmodium falciparum*: A Potential Route to Chemotherapy, *J. Med. Chem.* **2001**, *44* (6), 909-916.
20. Sanders, J. M.; Ghosh, S.; Chan, J. M. W.; Meints, G.; Wang, H.; Raker, A. M.; Song, Y.; Colantino, A.; Burzynska, A.; Kafarski, P.; Morita, C. T.; Oldfield, E., Quantitative Structure–Activity Relationships for $\gamma\delta$ T Cell Activation by Bisphosphonates, *J. Med. Chem.* **2004**, *47* (2), 375-384.
21. Lolli, M. L.; Rolando, B.; Tosco, P.; Chaurasia, S.; Stilo, A. D.; Lazzarato, L.; Gorassini, E.; Ferracini, R.; Oliaro-Bosso, S.; Fruttero, R.; Gasco, A., Synthesis and preliminary pharmacological characterisation of a new class of nitrogen-containing bisphosphonates (N-BPs), *Bioorg. Med. Chem.* **2010**, *18* (7), 2428-2438.

22. R. Hudson, H.; J. Wardle, N.; W.A. Bligh, S.; Greiner, I.; Grun, A.; Keglevich, G., N-Heterocyclic Dronic Acids: Applications and Synthesis, *Mini-Rev. Med. Chem.* **2012**, *12* (4), 313-325.
23. Nagy, D. I.; Grun, A.; Pavela, O.; Garadnay, S.; Greiner, I.; Keglevich, G., Efficient Synthesis of Ibandronate in the Presence of an Ionic Liquid, *Lett Drug Des Discov* **2018**, *15* (7), 713-720.
24. Zhang, Y.; Cao, R.; Yin, F.; Lin, F.-Y.; Wang, H.; Krysiak, K.; No, J.-H.; Mukkamala, D.; Houlihan, K.; Li, J.; Morita, C. T.; Oldfield, E., Lipophilic Pyridinium Bisphosphonates: Potent $\gamma\delta$ T Cell Stimulators, *Angew. Chem., Int. Ed.* **2010**, *49* (6), 1136-1138.
25. Idrees, A. S. M.; Sugie, T.; Inoue, C.; Murata-Hirai, K.; Okamura, H.; Morita, C. T.; Minato, N.; Toi, M.; Tanaka, Y., Comparison of $\gamma\delta$ T cell responses and farnesyl diphosphate synthase inhibition in tumor cells pretreated with zoledronic acid, *Cancer Sci.* **2013**, *104* (5), 536-542.
26. Sarafionos, S.G.; Kortz, U.; Pope, M.T.; Modak, M.J., Mechanism of polyoxometalate-mediated inactivation of DNA polymerases: an analysis with HIV-1 reverse transcriptase indicates specificity for the DNA-binding cleft, *Biochem J* **1996**, *319* (2), 619-626.
27. Boulmier, A.; Feng, X.; Oms, O.; Mialane, P.; Rivière, E.; Shin, C. J.; Yao, J.; Kubo, T.; Furuta, T.; Oldfield, E.; Dolbecq, A., Anticancer Activity of Polyoxometalate-Bisphosphonate Complexes: Synthesis, Characterization, In Vitro and In Vivo Results, *Inorg. Chem.* **2017**, *56* (13), 7558-7565.
28. Kortz, U.; Jameson, G. B.; Pope, M. T., Polyoxometalate Diphosphate Complexes. Folded Macrocyclic Dodecatungstates, $[(O_3PXPO_3)_4W_{12}O_{36}]^{16-}$ (X = O, CH₂), *J. Am. Chem. Soc.* **1994**, *116* (6), 2659-2660.
29. Kortz, U.; Pope, M. T., Polyoxometalate-Diphosphate Complexes. 3. Possible Intermediates in the Molybdate-Catalyzed Hydrolysis of Pyrophosphate. The Structure of

Hexamolybdomethylenediphosphonate, $[(O_3PCH_2PO_3)Mo_6O_{18}(H_2O)_4]^{4-}$, *Inorg. Chem.* **1995**, *34* (8), 2160-2163.

30. Kortz, U.; Pope, M. T., Polyoxometalate-Diphosphate Complexes. 4. Structure of $Na_4[(O_3PCHN(CH_3)_2PO_3)W_2O_6] \cdot 11H_2O$, *Inorg. Chem.* **1995**, *34* (14), 3848-3850.

31. Niu, J.; Zhang, X.; Yang, D.; Zhao, J.; Ma, P.; Kortz, U.; Wang, J., Organodiphosphonate-Functionalized Lanthanopolyoxomolybdate Cages, *Chem. Eur. J.* **2012**, *18* (22), 6759-6762.

32. Yang, L.; Ma, P.; Zhang, X.; Niu, J.; Wang, J., An organic–inorganic hybrid Dy(III)-containing polyoxomolybdate based on functionalized diphosphonate ligands, *Inorg. Chem. Commun.* **2013**, *35*, 5-8.

33. El Moll, H.; Dolbecq, A.; Mbomekalle, I. M.; Marrot, J.; Deniard, P.; Dessapt, R.; Mialane, P., Tuning the Photochromic Properties of Molybdenum Bisphosphonate Polyoxometalates, *Inorg. Chem.* **2012**, *51* (4), 2291-2302.

34. Yang, L.; Zhou, Z.; Ma, P.; Wang, J.; Niu, J., Assembly of Dimeric and Tetrameric Complexes of Polyoxomolybdo-bisphosphonates Built from $[(Mo_3O_8)\{O_3PC(O)(CH_2-3-C_5NH_5)PO_3\}]^{2-}$ Subunits, *Cryst. Growth Des.* **2013**, *13* (6), 2540-2547.

35. Compain, J.-D.; Mialane, P.; Marrot, J.; Sécheresse, F.; Zhu, W.; Oldfield, E.; Dolbecq, A., Tetra- to Dodecanuclear Oxomolybdate Complexes with Functionalized Bisphosphonate Ligands: Activity in Killing Tumor Cells, *Chem. Eur. J.* **2010**, *16* (46), 13741-13748.

36. Compain, J.-D.; Dolbecq, A.; Marrot, J.; Mialane, P.; Sécheresse, F., Characterization of tetra, dodeca and tetradeca Mo^V polyoxometalate wheels structured by etidronate ligands, *C R Chim* **2010**, *13* (3), 329-335.

37. El Moll, H.; Kemmegne-Mbougouen, J. C.; Haouas, M.; Taulelle, F.; Marrot, J.; Cadot, E.; Mialane, P.; Floquet, S.; Dolbecq, A., Syntheses, characterizations and properties of $[Mo_2O_2S_2]^{-}$

based oxothiomolybdenum wheels incorporating bisphosphonate ligands, *Dalton Trans.* **2012**, *41* (33), 9955-9963.

38. Oms, O.; Benali, T.; Marrot, J.; Mialane, P.; Puget, M.; Serier-Brault, H.; Deniard, P.; Dessapt, R.; Dolbecq, A., Fully Oxidized and Mixed-Valent Polyoxomolybdates Structured by Bisphosphonates with Pendant Pyridine Groups: Synthesis, Structure and Photochromic Properties, *Inorganics* **2015**, *3* (2), 279-294.

39. Tan, H.-Q.; Chen, W.-L.; Liu, D.; Li, Y.-G.; Wang, E.-B., Spontaneous resolution of a new diphosphonate-functionalized polyoxomolybdate, *Cryst. Eng. Comm.* **2010**, *12* (12), 4017-4019.

40. Banerjee, A.; Bassil, B. S.; Rösenthaller, G.-V.; Kortz, U., Fluorine Tagging of Polyoxometalates: The Cyclic $[\{\text{Mo}^{\text{V}}_2\text{O}_4(\text{H}_2\text{O})\}_4\{\text{O}_3\text{PC}(\text{CF}_3)(\text{O})\text{PO}_3\}_4]^{12-}$, *Eur. J. Inorg. Chem.* **2010**, *2010* (25), 3915-3919.

41. Banerjee, A.; Raad, F. S.; Vankova, N.; Bassil, B. S.; Heine, T.; Kortz, U., Polyoxomolybdodiphosphonates: Examples Incorporating Ethylidenepyridines, *Inorg. Chem.* **2011**, *50* (22), 11667-11675.

42. Tan, H.; Chen, W.; Liu, D.; Li, Y.; Wang, E., Two new cantilever-type polyoxometalates constructed from $\{\text{Mo}_2\text{O}_4\}^{2+}$ fragments and diphosphonates, *Dalton Trans.* **2010**, *39* (5), 1245-1249.

43. Saad, A.; Rousseau, G.; El Moll, H.; Oms, O.; Mialane, P.; Marrot, J.; Parent, L.; Mbomekallé, I.-M.; Dessapt, R.; Dolbecq, A., Molybdenum Bisphosphonates with Cr(III) or Mn(III) Ions, *J. Clust. Sci.* **2014**, *25* (3), 795-809.

44. Saad, A.; Zhu, W.; Rousseau, G.; Mialane, P.; Marrot, J.; Haouas, M.; Taulelle, F.; Dessapt, R.; Serier-Brault, H.; Rivière, E.; Kubo, T.; Oldfield, E.; Dolbecq, A., Polyoxomolybdate

Bisphosphonate Heterometallic Complexes: Synthesis, Structure, and Activity on a Breast Cancer Cell Line, *Chem. Eur. J.* **2015**, *21* (29), 10537-10547.

45. Zhang, L.; Sun, J.; Zhou, Y.; ul Hassan, S.; Wang, E.; Shi, Z., A general synthesis approach in action: preparation and characterization of polyoxomolybdenum(VI) organophosphonates through oxidative Mo–Mo bond cleavage in $\{\text{Mo}^{\text{V2}}\text{O}_4\}$, *Cryst. Eng. Comm.* **2012**, *14* (14), 4826-4833.

46. Xu, Q.; Sun, X.; Hu, F.; Wan, R.; Singh, V.; Ma, P.; Niu, J.; Wang, J., Two New Sandwich-Type Polyoxomolybdates Functionalized with Diphosphonates: Efficient and Selective Oxidation of Sulfides to Sulfones, *Materials* **2017**, *10* (10), 1173.

47. Sun, X.; Ban, R.; Ma, P.; Wang, J.; Zhang, D.; Niu, J.; Wang, J., Four transition-metal-bridging risedronate-based polyoxomolybdates: Syntheses, structures, characterizations and magnetic properties, *Synth. Met.* **2017**, *223*, 19-25.

48. Rousseau, G.; Zhang, S.; Oms, O.; Dolbecq, A.; Marrot, J.; Liu, R.; Shang, X.; Zhang, G.; Keita, B.; Mialane, P., Sequential Synthesis of 3 d–3 d, 3 d–4 d, and 3 d–5 d Hybrid Polyoxometalates and Application to the Electrocatalytic Oxygen Reduction Reactions, *Chem. Eur. J.* **2015**, *21* (34), 12153-12160.

49. Saad, A.; Anwar, N.; Rousseau, G.; Mialane, P.; Marrot, J.; Haouas, M.; Taulelle, F.; McCormac, T.; Dolbecq, A., Covalent Attachment of Thiophene Groups to Polyoxomolybdates or Polyoxotungstates for the Formation of Hybrid Films, *Eur. J. Inorg. Chem.* **2015**, *2015* (28), 4775-4782.

50. El Moll, H.; Dolbecq, A.; Marrot, J.; Rousseau, G.; Haouas, M.; Taulelle, F.; Rogez, G.; Wernsdorfer, W.; Keita, B.; Mialane, P., A Stable Hybrid Bisphosphonate Polyoxometalate Single-Molecule Magnet, *Chem. Eur. J.* **2012**, *18* (13), 3845-3849.

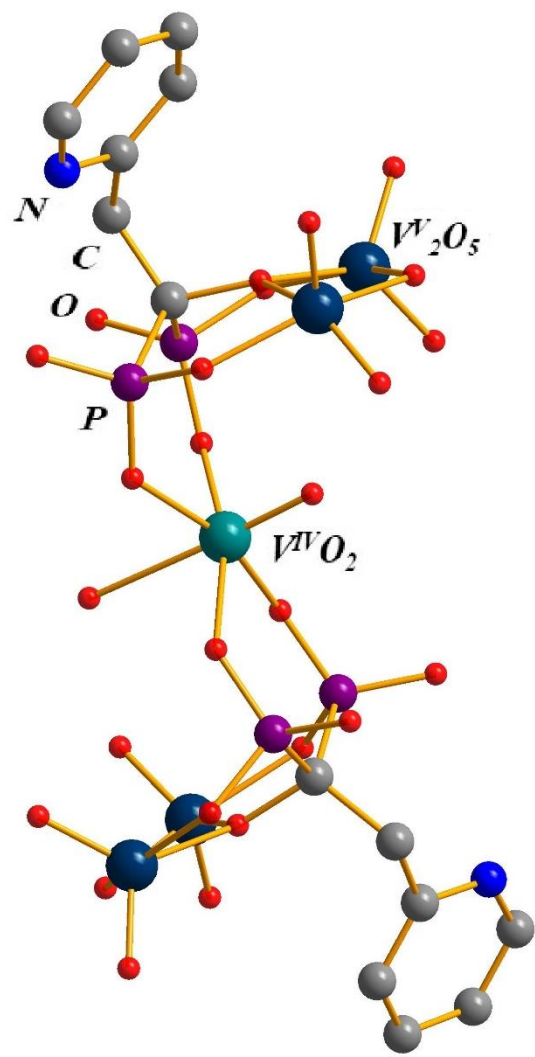
51. Zhang, Y.; Han, X.-B.; Zhang, Z.-M.; Liu, Z.-J.; Wang, E.-B., A {Ni₇} cluster-containing sandwich-type phosphotungstate functionalized by organic bisphosphonate ligands and its two-dimensional supramolecular structure, *Chin Chem Lett* **2013**, *24* (7), 581-584.
52. Paille, G.; Boulmier, A.; Bensaid, A.; Ha-Thi, M.-H.; Tran, T.-T.; Pino, T.; Marrot, J.; Rivière, E.; Hendon, C. H.; Oms, O.; Gomez-Mingot, M.; Fontecave, M.; Mellot-Draznieks, C.; Dolbecq, A.; Mialane, P., An unprecedented {Ni₁₄SiW₉} hybrid polyoxometalate with high photocatalytic hydrogen evolution activity, *Chem. Commun.* **2019**, *55* (29), 4166-4169.
53. El Moll, H.; Rousseau, G.; Dolbecq, A.; Oms, O.; Marrot, J.; Haouas, M.; Taulelle, F.; Rivière, E.; Wernsdorfer, W.; Lachkar, D.; Lacôte, E.; Keita, B.; Mialane, P., Properties of a Tunable Multinuclear Nickel Polyoxotungstate Platform, *Chem. Eur. J.* **2013**, *19* (21), 6753-6765.
54. Oms, O.; Yang, S.; Salomon, W.; Marrot, J.; Dolbecq, A.; Rivière, E.; Bonnefont, A.; Ruhlmann, L.; Mialane, P., Heteroanionic Materials Based on Copper Clusters, Bisphosphonates, and Polyoxometalates: Magnetic Properties and Comparative Electrocatalytic NO_x Reduction Studies, *Inorg. Chem.* **2016**, *55* (4), 1551-1561.
55. Ban, R.; Sun, X.; Wang, J.; Ma, P.; Zhang, C.; Niu, J.; Wang, J., Polyoxotungstate incorporating organotriphosphonate ligands and lanthanide ions: syntheses, characterization, magnetism and photoluminescence properties, *Dalton Trans.* **2017**, *46* (18), 5856-5863.
56. El Moll, H.; Zhu, W.; Oldfield, E.; Rodriguez-Albelo, L. M.; Mialane, P.; Marrot, J.; Vila, N.; Mbomekallé, I. M.; Rivière, E.; Duboc, C.; Dolbecq, A., Polyoxometalates Functionalized by Bisphosphonate Ligands: Synthesis, Structural, Magnetic, and Spectroscopic Characterizations and Activity on Tumor Cell Lines, *Inorg. Chem.* **2012**, *51* (14), 7921-7931.

57. Aleksandrov, G. G.; Sergienko, V. S.; Afonin, E. G., Crystal structure of disordered diethylammonium oxo(1-hydroxoethane-1,1-diphosphonato)vanadate(IV) hydrate, *Crystallogr. Rep.* **2001**, *46* (1), 46-50.
58. Ban, R.; Liang, Y.; Ma, P.; Zhang, D.; Niu, J.; Wang, J., Synthesis, crystal structure, characterization and magnetic property of a new organophosphonate-based polyoxovanadate, *Inorg. Chem. Commun.* **2016**, *71*, 65-67.
59. Rocha, J.; Almeida Paz, F. A.; Shi, F.-N.; Ferreira, R. A. S.; Trindade, T.; Carlos, L. D., Photoluminescent Porous Modular Lanthanide–Vanadium–Organic Frameworks, *Eur. J. Inorg. Chem.* **2009**, (33), 4931.
60. Tomane, S.; López-Maya, E.; Boujday, S.; Humblot, V.; Marrot, J.; Rabasso, N.; Castells-Gil, J.; Sicard, C.; Dolbecq, A.; Mialane, P.; Vallée, A., One-pot synthesis of a new generation of hybrid bisphosphonate polyoxometalate gold nanoparticles as antibiofilm agents, *Nanoscale Advances* **2019**, *1* (9), 3400-3405.
61. Keene, T. D.; D'Alessandro, D. M.; Krämer, K. W.; Price, J. R.; Price, D. J.; Decurtins, S.; Kepert, C. J., $[V_{16}O_{38}(CN)]^{9-}$: A Soluble Mixed-Valence Redox-Active Building Block with Strong Antiferromagnetic Coupling, *Inorg. Chem.* **2012**, *51* (17), 9192-9199.
62. Brisdon, A., Kazuo Nakamoto Infrared and Raman Spectra of Inorganic and Coordination Compounds, Part B, Applications in Coordination, Organometallic, and Bioinorganic Chemistry, 6th edn Wiley, 2009, 424 pp. (hardback) ISBN 978-0-471-74493-1, *Applied Organometallic Chemistry* **2010**, *24* (6), 489-489.
63. Chen, S.; Liu, Y.; Guo, J.; Li, P.; Huo, Z.; Ma, P.; Niu, J.; Wang, J., A multi-component polyoxometalate and its catalytic performance for CO₂ cycloaddition reactions, *Dalton Trans.* **2015**, *44* (22), 10152-10155.

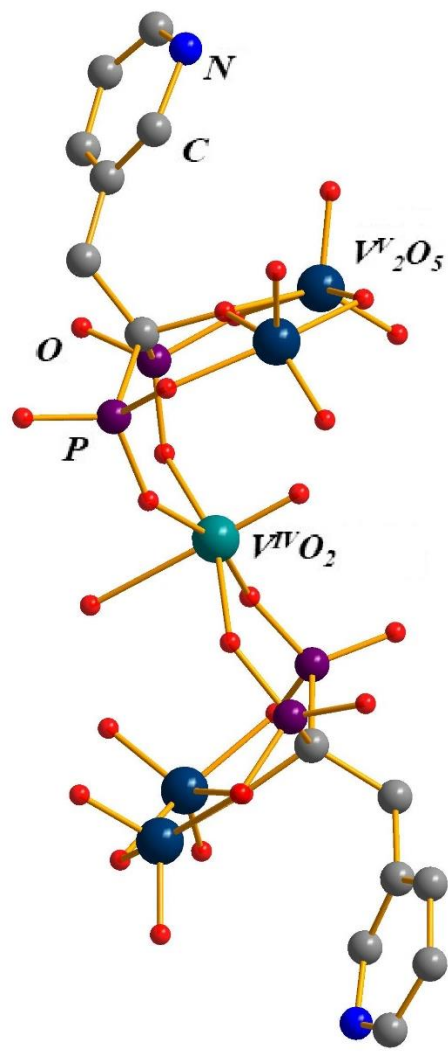
64. Arichi, J.; Pereira, M. M.; Esteves, P. M.; Louis, B., Synthesis of Keggin-type polyoxometalate crystals, *Solid State Sci.* **2010**, *12* (11), 1866-1869.
65. Kurbah, S. D.; Kumar, A.; Syiemlieh, I.; Lal, R. A., Pi-pi interaction and hydrogen bonding in crystal structure of vanadium(V) complex containing mono hydrazone ligand: Synthesis and protein binding studies, *Inorg. Chem. Commun.* **2017**, *86*, 6-9.
66. Mirdya, S.; Roy, S.; Chatterjee, S.; Bauzá, A.; Frontera, A.; Chattopadhyay, S., Importance of π -Interactions Involving Chelate Rings in Addition to the Tetrel Bonds in Crystal Engineering: A Combined Experimental and Theoretical Study on a Series of Hemi- and Holodirected Nickel(II)/Lead(II) Complexes, *Cryst. Growth Des.* **2019**, *19* (10), 5869-5881.
67. Zabierowski, P.; Szklarzewicz, J.; Gryboś, R.; Modryl, B.; Nitek, W., Assemblies of salen-type oxidovanadium(IV) complexes: substituent effects and in vitro protein tyrosine phosphatase inhibition, *Dalton Trans.* **2014**, *43* (45), 17044-17053.
68. Biswal, D.; Pramanik, N. R.; Chakrabarti, S.; Drew, M. G. B.; Acharya, K.; Chandra, S., Syntheses, crystal structures, DFT calculations, protein interaction and anticancer activities of water soluble dipicolinic acid-imidazole based oxidovanadium(IV) complexes, *Dalton Trans.* **2017**, *46* (47), 16682-16702.
69. Rehder, D., *Bioinorganic Vanadium Chemistry*. John Wiley & Sons, Ltd.: 2008.
70. Huang, Y.; Ren, J.; Qu, X., Nanozymes: Classification, Catalytic Mechanisms, Activity Regulation, and Applications, *Chem. Rev.* **2019**, *119* (6), 4357-4412.
71. Gao, L.; Zhuang, J.; Nie, L.; Zhang, J.; Zhang, Y.; Gu, N.; Wang, T.; Feng, J.; Yang, D.; Perrett, S.; Yan, X., Intrinsic peroxidase-like activity of ferromagnetic nanoparticles, *Nat. Nanotechnol* **2007**, *2* (9), 577-583.

72. Bhattacharyya, S.; Ali, S. R.; Venkateswarulu, M.; Howlader, P.; Zangrando, E.; De, M.; Mukherjee, P. S., Self-Assembled Pd₁₂ Coordination Cage as Photoregulated Oxidase-Like Nanozyme, *J. Am. Chem. Soc.* **2020**, *142* (44), 18981-18989.
73. Sun, H.; Gao, N.; Dong, K.; Ren, J.; Qu, X., Graphene Quantum Dots-Band-Aids Used for Wound Disinfection, *ACS Nano* **2014**, *8* (6), 6202-6210.
74. Xu, B. L.; Wang, H.; Wang, W. W.; Gao, L. Z.; Li, S. S.; Pan, X. T.; Wang, H. Y.; Yang, H. L.; Meng, X. Q.; Wu, Q. W.; Zheng, L. R.; Chen, S. M.; Shi, X. H.; Fan, K. L.; Yan, X. Y.; Liu, H. Y., A Single-Atom Nanozyme for Wound Disinfection Applications, *Angew. Chem., Int. Ed.* **2019**, *58* (15), 4911-4916.
75. Yin, W. Y.; Yu, J.; Lv, F. T.; Yan, L.; Zheng, L. R.; Gu, Z. J.; Zhao, Y. L., Functionalized Nano-MoS₂ with Peroxidase Catalytic and Near-Infrared Photothermal Activities for Safe and Synergetic Wound Antibacterial Applications, *ACS Nano* **2016**, *10* (12), 11000-11011.
76. Labas, M. D.; Zalazar, C. S.; Brandi, R. J.; Cassano, A. E., Reaction kinetics of bacteria disinfection employing hydrogen peroxide, *Biochem. Eng. J.* **2008**, *38* (1), 78-87.
77. Gao, L. Z.; Giglio, K. M.; Nelson, J. L.; Sondermann, H.; Travis, A. J., Ferromagnetic nanoparticles with peroxidase-like activity enhance the cleavage of biological macromolecules for biofilm elimination, *Nanoscale* **2014**, *6* (5), 2588-2593.
78. Liu, S. B.; Zeng, T. H.; Hofmann, M.; Burcombe, E.; Wei, J.; Jiang, R. R.; Kong, J.; Chen, Y., Antibacterial Activity of Graphite, Graphite Oxide, Graphene Oxide, and Reduced Graphene Oxide: Membrane and Oxidative Stress, *ACS Nano* **2011**, *5* (9), 6971-6980.
79. Huang, L.; Chen, J. X.; Gan, L. F.; Wang, J.; Dong, S. J., Single-atom nanozymes, *Sci. Adv.* **2019**, *5* (5).

80. Ghosh, S.; Roy, P.; Karmodak, N.; Jemmis, E. D.; Mugesh, G., Nanoisozymes: Crystal-Facet-Dependent Enzyme-Mimetic Activity of V₂O₅ Nanomaterials, *Angew. Chem., Int. Ed.* **2018**, *57* (17), 4510-4515.
81. Singh, N.; NaveenKumar, S. K.; Geethika, M.; Mugesh, G., A Cerium Vanadate Nanozyme with Specific Superoxide Dismutase Activity Regulates Mitochondrial Function and ATP Synthesis in Neuronal Cells, *Angew. Chem., Int. Ed.* **2021**, *60* (6), 3121-3130.
82. Bijelic, A.; Aureliano, M.; Rompel, A., The antibacterial activity of polyoxometalates: structures, antibiotic effects and future perspectives, *Chem. Commun.* **2018**, *54* (10), 1153-1169.
83. Herrmann, S.; De Matteis, L.; de la Fuente, J. M.; Mitchell, S. G.; Streb, C., Removal of Multiple Contaminants from Water by Polyoxometalate Supported Ionic Liquid Phases (POM-SILPs), *Angew. Chem., Int. Ed.*, **2017**, *56* (6), 1667-1670.
84. Kubo, A.-L.; Kremer, L.; Herrmann, S.; Mitchell, S. G.; Bondarenko, O. M.; Kahru, A.; Streb, C., Antimicrobial Activity of Polyoxometalate Ionic Liquids against Clinically Relevant Pathogens, *ChemPlusChem* **2017**, *82* (6), 867-871.
85. Sheldrick, G., A short history of SHELX, *Acta Crystallogr.* **2008**, *64* (1), 112-122.
86. Sheldrick, G. M., Program for Empirical Absorption Correction of Area Detector Data, *SADABS* **1996**.
87. Srinivasa Rao, D. V. N.; Dandala, R.; Narayanan, G. K. A. S. S.; Lenin, R.; Sivakumaran, M.; Naidu, A., Novel Procedure for the Synthesis of 1-Hydroxo-1,1-bisphosphonic Acids using Phenols as Medium, *Synth. Commun.* **2007**, *37* (24), 4359-4365.
88. Cao, F. F.; Zhang, L.; Wang, H.; You, Y. W.; Wang, Y.; Gao, N.; Ren, J. S.; Qu, X. G., Defect-Rich Adhesive Nanozymes as Efficient Antibiotics for Enhanced Bacterial Inhibition, *Angew. Chem., Int. Ed.* **2019**, *58* (45), 16236-16242.



(a)



(b)

Figure 1.

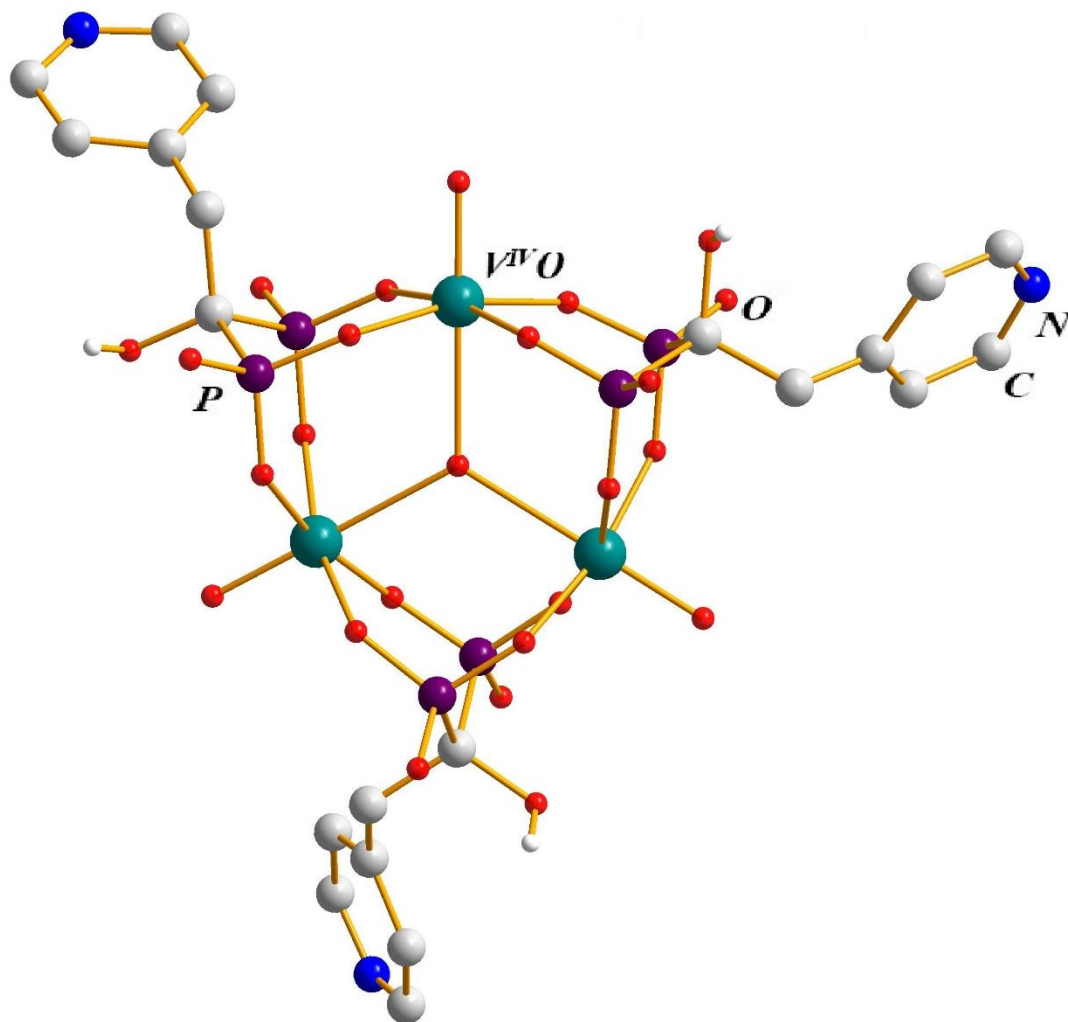


Figure 2.

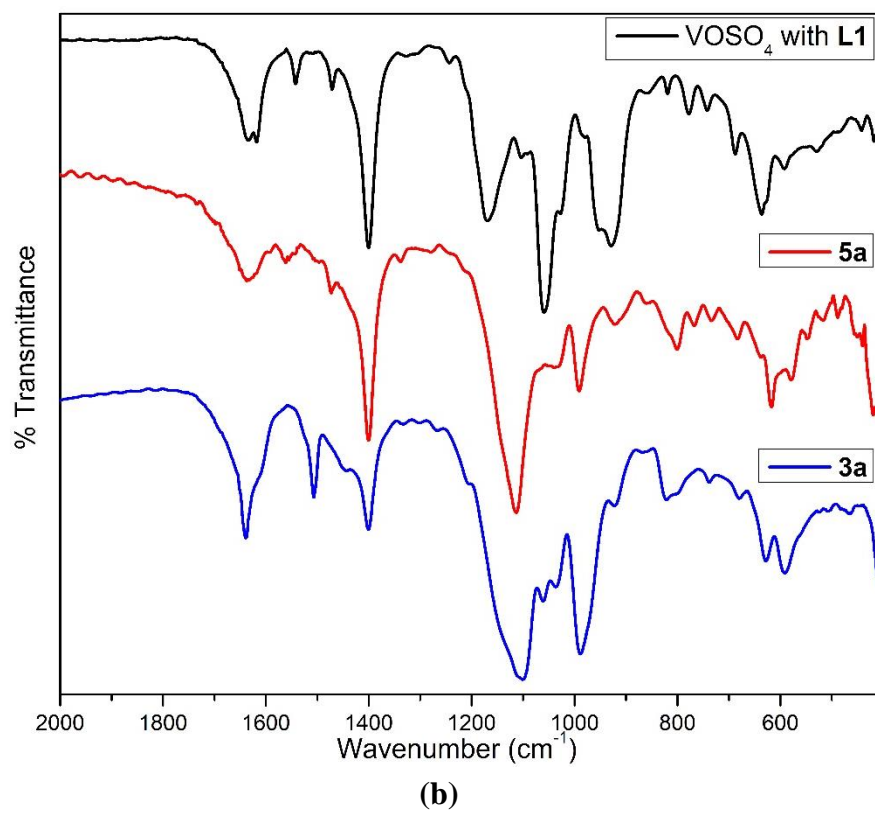
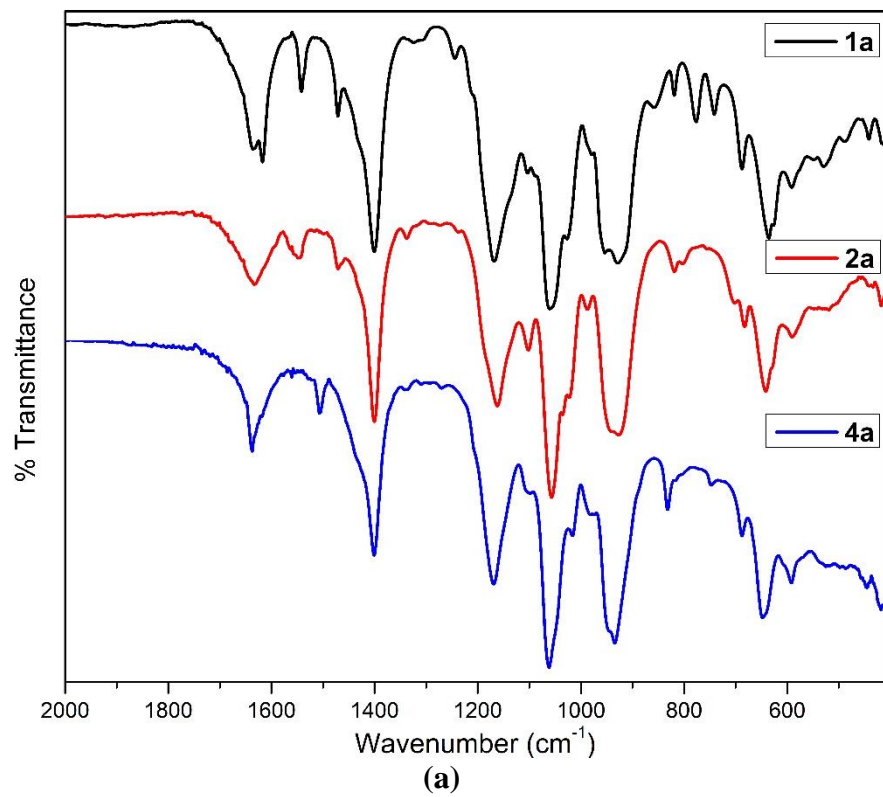


Figure 3.

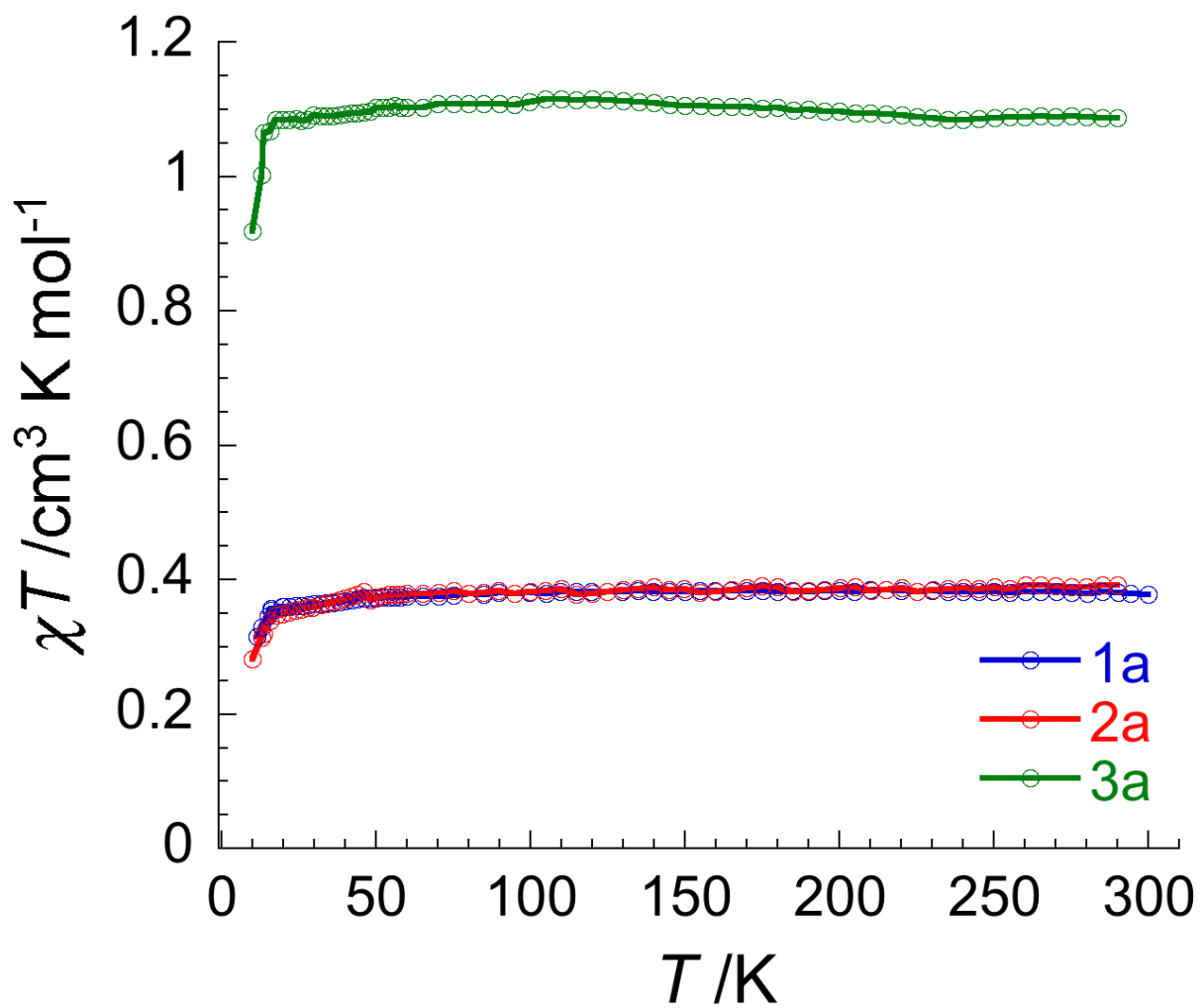


Figure 4.

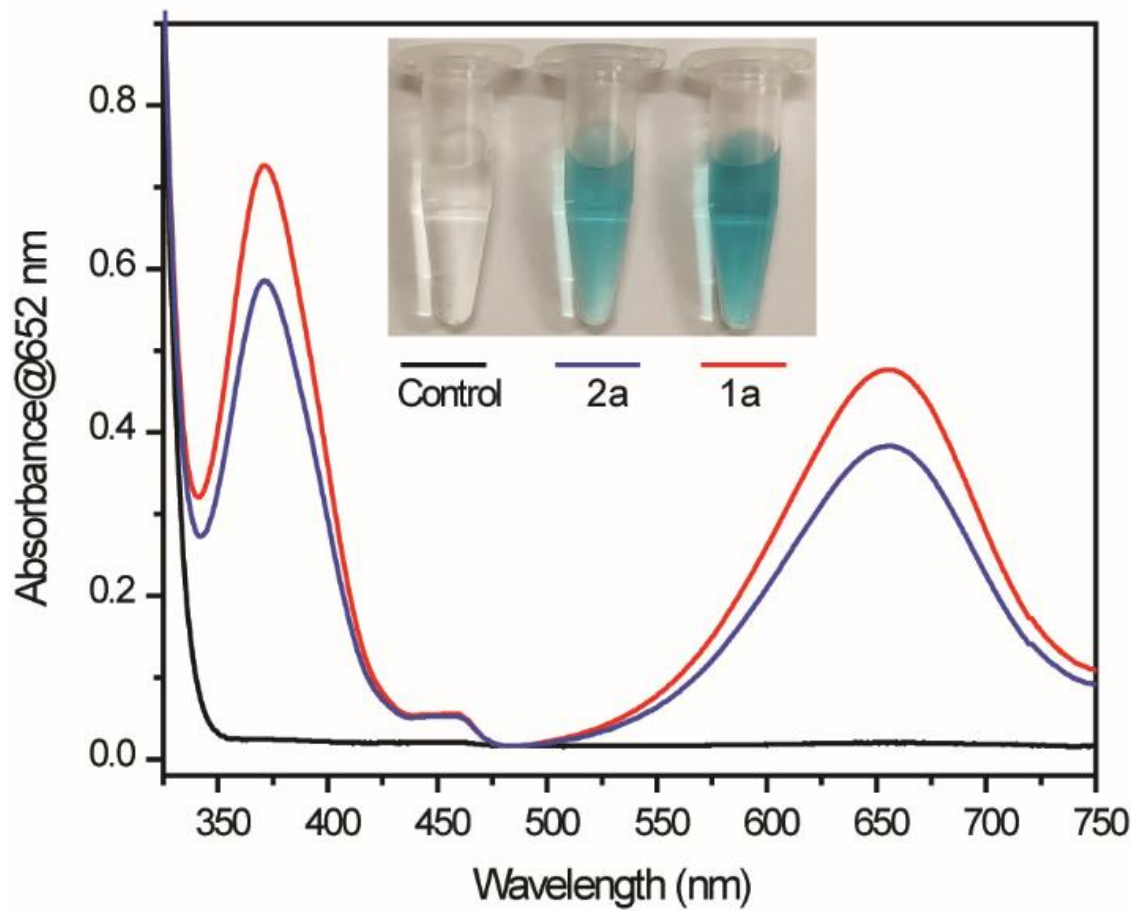


Figure 5.

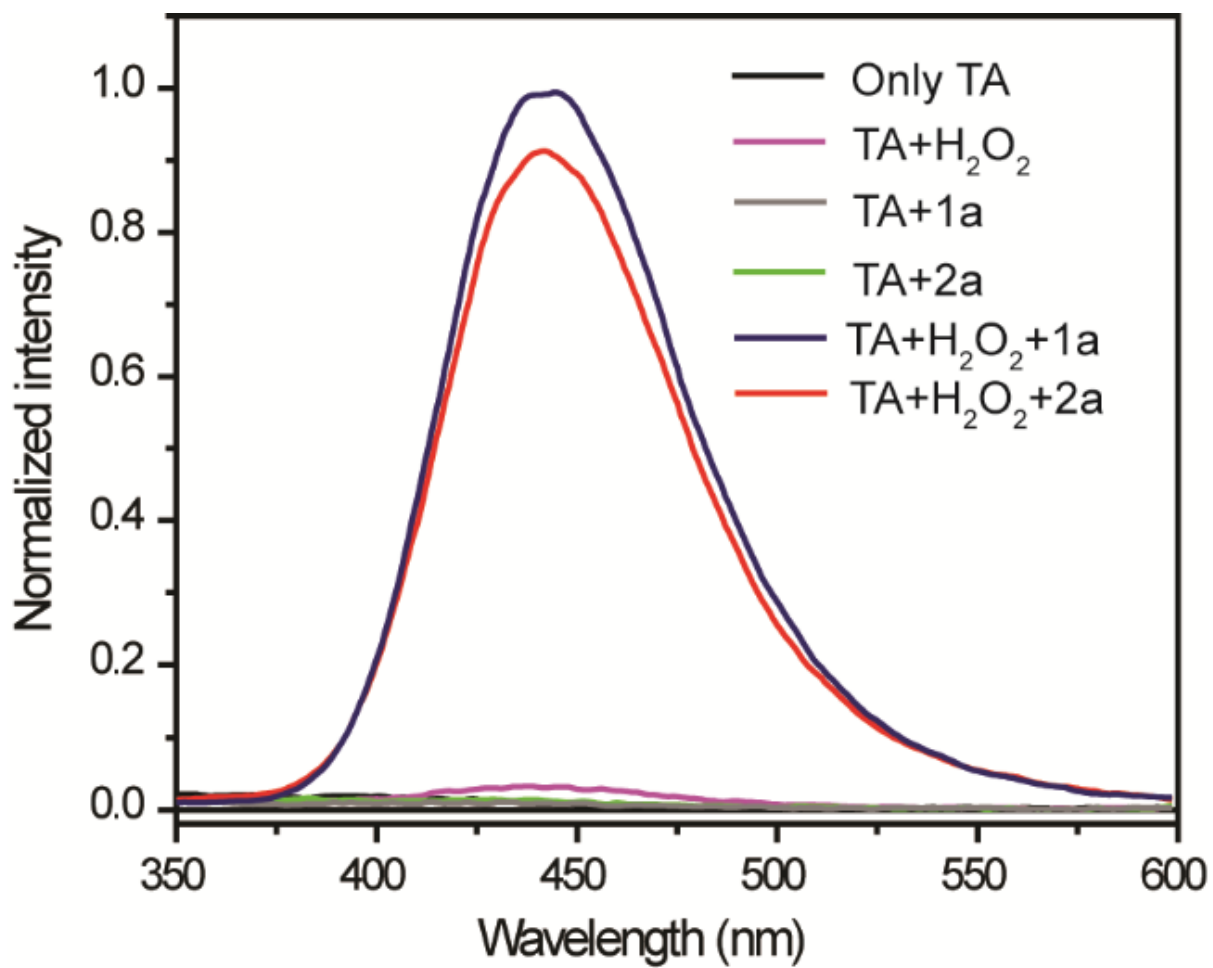


Figure 6.

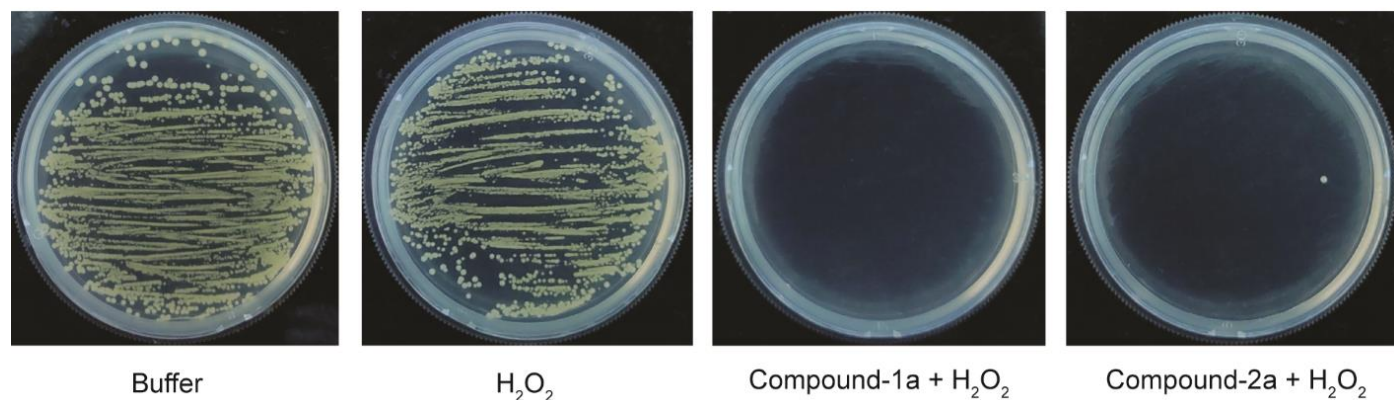


Figure 7.

FIGURE CAPTIONS:

Figure 1. Ball-and-stick representation of (a) polyanion **1**, $[(V^{IV}O_2)(V^V_2O_5)_2\{O_3P-C(O)(CH_2-2-C_5NH_4)-PO_3\}_2]^{10-}$, and (b) polyanion **2**, $[(V^{IV}O_2)(V^V_2O_5)_2\{O_3P-C(O)(CH_2-3-C_5NH_4)-PO_3\}_2]^{10-}$. Color code, Vanadium(V): Teal, Vanadium(IV): Green, Phosphorous: Magenta, Oxygen: Red, Nitrogen: Blue, Carbon: Grey, Hydrogen: white. Hydrogen atoms on carbon have been omitted for clarity.

Figure 2. Ball-and-stick representation of polyanion **3**, $[(V^{IV}O)_3(O)\{O_3PC(OH)(CH_2-4-C_5NH_4)-PO_3\}_3]^{8-}$. Color code, Vanadium(IV): Green, Phosphorous: Magenta, Oxygen: Red, Nitrogen: Blue, Carbon: Grey, Hydrogen: white. Hydrogen atoms on carbon have been omitted for clarity.

Figure 3. Comparative IR spectrum (fingerprint region only) for (a) compounds **1a**, **2a** and **4a**; and for (b) product obtained upon reaction of $VOSO_4$ with **L1**, and compounds **5a** and **3a**.

Figure 4. Temperature dependence of χT product for **1a**, **2a** and **3a** at 1000 Oe.

Figure 5. UV absorption plot of TMB (0.5 mM) in presence and absence of the compound **1a** and compound **2a** (50 $\mu\text{g/mL}$) with H_2O_2 (2.5 mM) after 1 hour.

Figure 6. Hydroxy radical ($\bullet\text{OH}$) detection assay using terephthalic acid (0.5 mM), H_2O_2 (5 mM) in presence of compounds **1a** and **2a** (100 $\mu\text{g/mL}$). The fluorescence spectra were recorded with the excitation wavelength 315 nm.

Figure 7. Images of bacterial colonies formed by MRSA bacteria after exposure of H_2O_2 (0.5 mM) in presence of compound **1a** (50 $\mu\text{g/mL}$) and compound **2a** (50 $\mu\text{g/mL}$) in acetate buffer medium (0.1 M, pH = 4.2) for 2h.

Polyoxovanadates with ethylidene-pyridine functionalized bisphosphonate ligands: Synthesis, Structure, Spectroscopic Characterization, Magnetic and Anti-Bacterial studies

Dewendra Thakre, Sk Rajab Ali, Sakshi Mehta, Noohul Alam, Masooma Ibrahim, Debajit Sarma,*
Abhishake Mondal, Mrinmoy De, and Abhishek Banerjee*

TOC text and graphic

We have prepared five new polyoxovanadate – bisphosphonate derivatives with ethylidene-pyridine functionalized bisphosphonate ligands. Reaction of V^{+5} compounds with bisphosphonate ligands gave a mixed-valent V^{IV}/V^V assembly of polyoxovanadate, while the reaction of V^{+4} compound with bisphosphonate ligands gave a reduced V^{IV} assembly of polyoxovanadate. The obtained compounds were characterized in the solid-state by single-crystal X-ray diffraction and magnetic studies, and in solution by NMR and UV-Vis spectroscopy. Anti-bacterial studies showed peroxidase-like activity for the compounds.

